OAK RIDGE NATIONAL LABORATORY
operated by
UNION CARBIDE CORPORATION
NUCLEAR DIVISION
for the
U.S. ATOMIC ENERGY COMMISSION

ORNL - TM - 2206

THERMAL-NEUTRON FLUX GENERATION BY HIGH-ENERGY PROTONS
(Thesis)

Wayne A. Coleman

A dissertation presented to the Graduate Council of the University of Tennessee in partial fulfillment of the requirements for the degree of Doctor of Philosophy.

ORNL-TM-2206

Contract No. W-7405-eng-26

Neutron Physics Division

THERMAL-NEUTRON FLUX GENERATION BY HIGH-ENERGY PROTONS*

Wayne A. Coleman

NOTE:

This work partially supported by
NATIONAL AERONAUTICS AND SPACE ADMINISTRATION
under Order R-104(1)

*A dissertation presented to the Graduate Council of the University of Tennessee in partial fulfillment of the requirements for the degree of Doctor of Philosophy.

JULY 1968

OAK RIDGE NATIONAL LABORATORY
Oak Ridge, Tennessee
operated by
UNION CARBIDE CORPORATION
for the
U. S. ATOMIC ENERGY COMMISSION

TABLE OF CONTENTS

LIST OF TABLES

LIST OF FIGURES

FIGURE PAGE

FIGURE PAGE

FIGURE PAGE

ABSTRACT

The research for this dissertation was performed in two general phases. The first phase consisted of revising NTC, a Monte Carlo computer code that calculates a description of proton and neutron transport below ∿450 MeV. Most importantly the revision includes an extension of the valid energy range to ∿3 BeV and a description of the production and transport of π and μ mesons. The basic code theory employed in NTC has been retained in the revised code NMTC. A discussion of the code theory incorporated in NMTC is given in the dissertation with emphasis on those aspects of the code which differ from NTC.

In the second phase of work, calculations were made using NMTC, and the results were compared with experimental thermal-neutron flux measurements to determine the validity of the code. In the experiments, accelerator protons ranging from 0.54 to 2.0 BeV were used to bombard thick targets of Be, Sn, Pb, and depleted U, which were surrounded by a large water tank. The thermal-neutron flux was measured as a function of position in the water moderator. The calculated thermal-neutron-flux distributions using NMTC are in quite good agreement with the experimental results.

The feasibility of producing an intense thermal-neutron flux from high-energy protons in thick targets has received considerable attention in recent years and was the motivation for the experimental measurements mentioned above with which the calculations were compared. Additional calculations have been carried out to obtain information concerning this

method of thermal-neutron-flux generation which is not available experimentally. These calculations included:

1. Thermal-neutron-flux distribution using a Pb target and a D_2O moderator;
2. Heat-producing energy release as a function of position in various targets;
3. Total heat-producing energy release in the target and moderator;
4. Neutron production as a function of position in a Pb target;
5. Thermal-neutron-flux distributions in a D_2O moderator using Pb targets of 5- and 10-cm radius;
6. Comparisons of thermal-neutron-flux distributions in various moderator configurations combining D_2O and H_2O, and using a Pb target.

From the data referred to in 4 and 5 above, observations are made regarding an appropriate shape for a Pb target using 900-MeV incident protons.

CHAPTER I

INTRODUCTION

When a high[1]-energy proton, neutron, or pion interacts with a nucleus, several secondary nucleons and pions may be produced. A number of these secondaries are likely to have energies which are sufficiently high enough to initiate similar productive events with other nuclei. In this way, a macroscopic particle cascade develops.

The nucleon transport code NTC (Kinney, 1964) was developed to determine various properties of such cascades in arbitrary, specified environments. Monte Carlo methods are employed in NTC to obtain a detailed description of a macroscopic nucleon cascade. However, pion production is neglected and the code is not designed to transport particles other than nucleons. In general, one cannot use NTC and expect to obtain an accurate description of particle transport when source particle energies exceed the practical threshold for pion production, which is approximately 450 MeV.

The first phase of work performed for this dissertation consisted of revising NTC to provide for pion production using the medium-energy collision code of Bertini (1963, 1967), which has recently become available, and to make provision in the revised code for transporting pions as well as the higher energy nucleons. Furthermore, the revised code, NMTC,

---

[1]High energies are regarded as being at or above the 20- to 50-MeV range.

also transports muons since these particles are produced by pion decay. Due to limitations in the Bertini collision code, the maximum energies for nucleons and pions that may be considered in NMTC are 3500 MeV and 2500 MeV, respectively. For struck nucleons, these energies correspond to the practical thresholds for ternary pion production by nucleons and double pion production by pions.

Recently there has been interest in producing a large thermal-neutron flux by using accelerator protons of the order of 1 BeV to bombard certain thick-target materials that are surrounded by an appropriate moderator. An experimental arrangement for producing a thermal-neutron flux using this general concept is usually referred to as an intense neutron generator and will hereinafter be referred to as an ING. To test the feasibility of the concept, a series of experiments was performed by Fraser et al. (1965) at Brookhaven National Laboratory. In these experiments, accelerator protons of fixed energies ranging from 0.54 to 2.0 BeV were used to bombard targets of Be, Sn, Pb, and depleted U. Measurements of the thermal-neutron flux were made at various positions in an H_2O moderator. The experimental geometry is illustrated in Figure 1.

In the second phase of dissertation work, NMTC was first used to obtain calculated results that could be compared with the experimental data obtained at Brookhaven. This was selected as a first application for the code because a) the comparisons with the experimental data provided a reasonably definitive test on the validity of the extended code, and b) if the comparisons with the experimental data were good, the code could be used to estimate other quantities associated with particle behavior in an ING for which experimental data were not available.

ORNL-DWG 68-2224

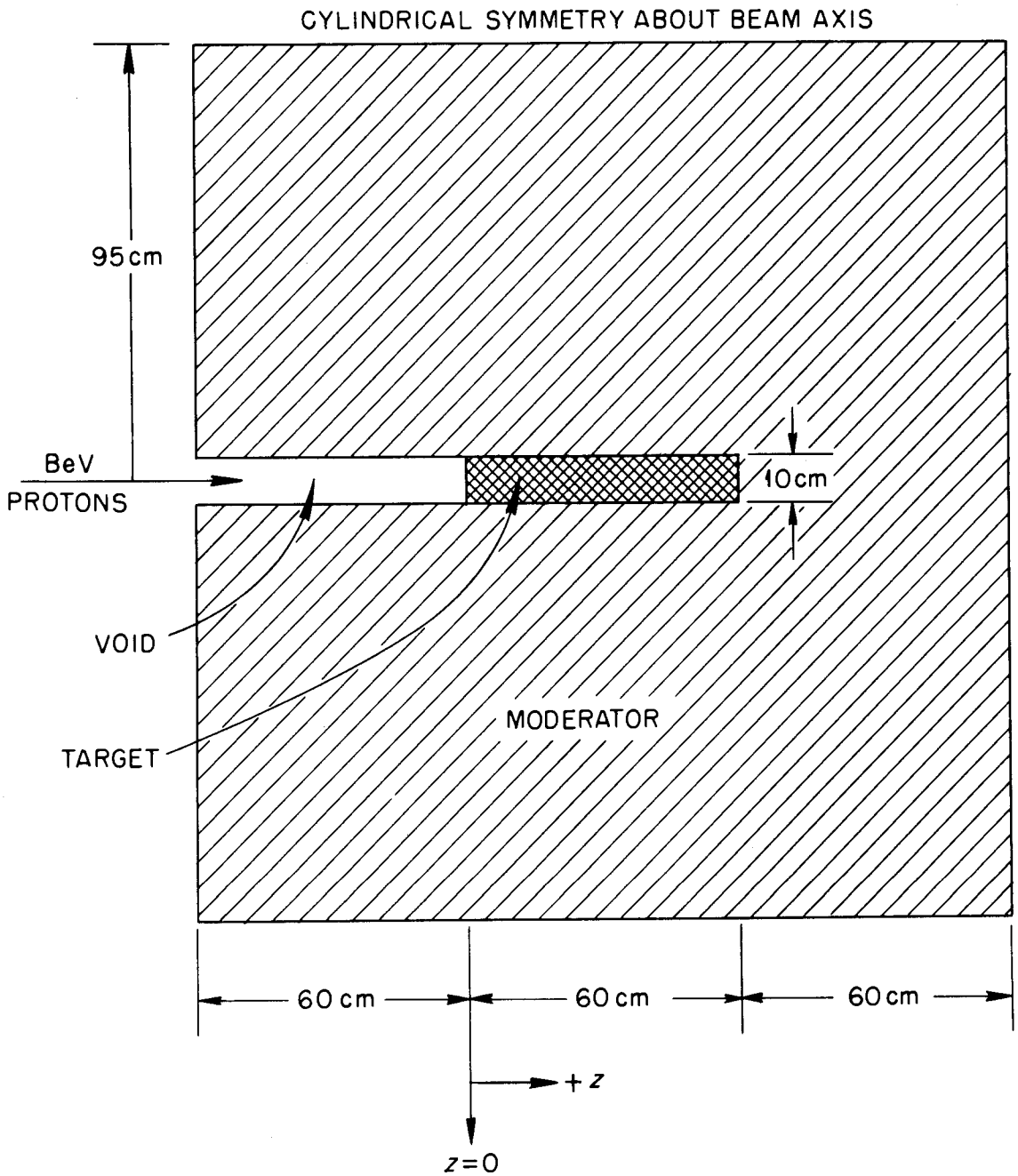

Figure 1. Schematic diagram of the ING concept: intense neutron generation via a proton accelerator.

Thermal-neutron flux distributions were calculated in a water moderator using targets of Be, Sn, Pb, and depleted U in combination with incident proton energies of 0.54, 0.75, 0.9, 1.5, and 2.0 BeV. The calculational geometry was identical to that given in Figure 1. Comparisons with experimental data[2] are given for 900- and 1500-MeV protons incident on Be, Sn, and U, and for Pb using protons at 540, 750, 900, 1500, and 2000 MeV.

In addition to the calculations for comparisons with experimental data, the following data were calculated:

1. Thermal-neutron-flux distributions in a D_2O moderator using a Pb target;
2. Heat-producing energy release as a function of position in various targets;
3. Total heat-producing energy release in the target and moderator;
4. Neutron production as a function of position in a Pb target;
5. Thermal-neutron-flux distributions in a D_2O moderator using Pb targets of 5- and 10-cm radius; and
6. Comparisons of thermal-neutron-flux distributions in various moderator configurations combining D_2O and H_2O and using a Pb target.

[2]All of the experimental data were not published (Fraser et al., 1965). The author is grateful to Dr. Alexander Zucker of the Oak Ridge National Laboratory, who was a member of the experimental group at Brookhaven, for providing the unpublished data.

CHAPTER II

THE NUCLEON-MESON TRANSPORT CODE

I. GENERAL SCHEME OF OPERATION

NMTC is a FORTRAN IV computer code written for the IBM 360/75 computer. The code employs Monte Carlo methods to compute descriptions of the transport of nucleons up to 3.5 BeV, pions up to 2.5 BeV, and muons of 2.5 BeV. NMTC consists of two basic transport codes: NMT and a modified version of 05R (Irving et al., 1965). Virtually arbitrary geometries may be specified in NMT and 05R through Irving's (1965) general geometry routines. The normal flow of information is shown in Figure 2. Particles are introduced into the system in NMT and transported to an appropriate cutoff energy that is usually in the energy region between 20 and 50 MeV. The cutoff energy, which is discussed in section II of this chapter, is imposed principally by limitations in nuclear collision theory. Neutrons appearing below the NMT cutoff are transported via the 05R code. Charged particles are not transported below this cutoff.

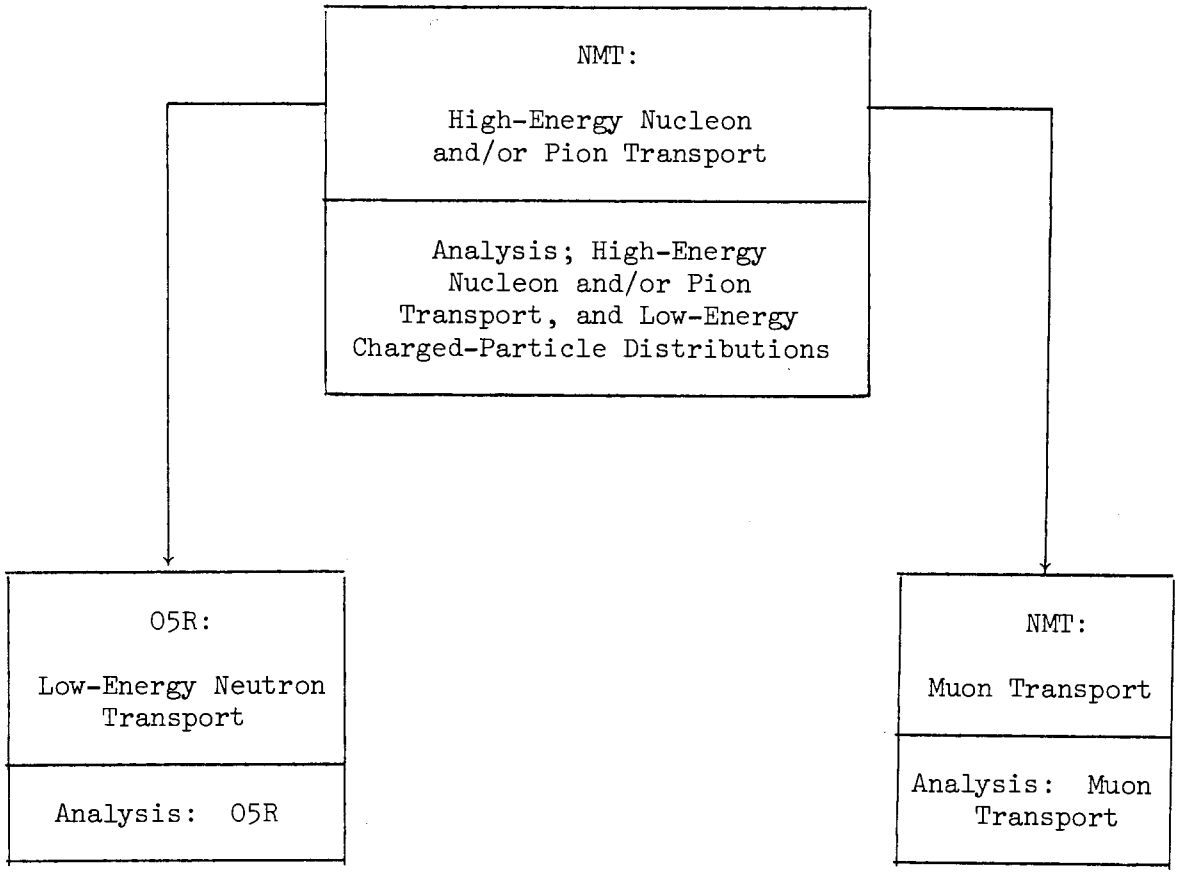

Figure 2. Normal flow of information in NMTC.

Each sample history begins by selecting a source particle position, direction, energy, type, and statistical weight. A tentative particle flight trajectory is selected from a cumulative distribution function having the form

$$\int_0^S {}_k\Sigma_m\,[E_{k,m}(s;E_o)]\; e^{-\int_0^s {}_k\Sigma_m[E_{k,m}(s';E_o)]\,ds'}\,ds,\quad 0 \le S\ , \qquad \text{II-1}$$

where E_o is the particle kinetic energy at the beginning of the flight, $E_{k,m}(s;E_o)$ is the particle kinetic energy after traveling a distance s from the last event, and ${}_k\Sigma_m[E_{k,m}(s;E_o)]$ is the total cross section for a nuclear event in inverse centimeters. The subscripts k and m denote the particle type and material, respectively.

Using the selected flight trajectory, it is determined if the particle has either crossed a medium boundary or, for charged particles, slowed past the cutoff energy. If an external medium boundary is encountered so that the particle has escaped the system or if the cutoff energy has been reached, then a description of the event is recorded, and NMT proceeds to transport the next descendant. If an internal medium boundary is encountered, the particle energy at the crossing is calculated, the event is recorded, and a flight trajectory is selected in the new medium. If the particle has neither reached the energy cutoff nor crossed a medium boundary, then a collision site has been selected, and a complete description of the interaction products will be determined using the nuclear

interaction model which is described in section II of this chapter. When all of the descendants of the current cascade have been transported, the code introduces the next source particle. The calculation continues until the desired number of sample histories is attained.

Normally the output of NMT is saved on two magnetic tapes. One of the tapes contains detailed information on the nucleon and pion histories. In addition to information on the transported particles, a description of the residual nuclei and the charged particles produced below the energy cutoff is also given. Information may be read from this tape and processed in an analysis code written by the user. A subsequent NMT calculation is made to transport the muons resulting from pion decay. The muon source distributions are read directly from the nucleon-pion history tape. The second output tape from a nucleon-pion transport calculation contains a description of the neutrons appearing in the system below the NMT cutoff energy and is used as a source for neutron transport in 05R. Generally, the output of 05R and the muon transport are written on tape and processed in separate analysis codes that are written by the user. A general discussion of the 05R code is a digression and will not be given in this dissertation. A detailed account of the theory and operation of 05R is given by Irving et al. (1965). Normally the treatment of nonelastic collisions in 05R is left to the discretion of the user. In the NMTC version of 05R, nonelastic collisions are treated using direct compound nucleus formation followed by nuclear evaporation.

II. NUCLEAR COLLISION THEORY

The Cascade-Evaporation Model

A description of nuclear collision products is obtained in NMT by employing the intranuclear-cascade code of Bertini (1963, 1967). Elastic collisions in NMT are neglected since the angular distributions of the scattered particles are extremely forward for most nuclei. Neither the cascade-evaporation model nor the exclusion of elastic scattering applies to collisions with hydrogen nuclei. These events are treated separately in NMT, and a discussion of them is deferred until later in this section. The details of the models used in the intranuclear calculations and in the evaporation calculations are not included in the subject matter of this dissertation. However, a brief description of the models used in these calculations will be given to provide some understanding of how descriptions of the nuclear collision products are obtained.

The intranuclear calculations are performed using BERT, a subprogram version of Bertini's medium-energy intranuclear-cascade code (1967). The model used in BERT assumes that a nonelastic interaction with a nucleus may be described in terms of individual particle-particle collisions occurring within the nucleus and that the kinematics of these collisions are not influenced by the remaining nucleon population. Spatial variations of the nucleon energy spectrum, the nucleon number density, and the nucleon potential are taken into account. Free particle-particle cross sections are used in tracking particles within the nucleus.

An incident particle may collide with one of the nucleons or pass uncollided through the nucleus. If a collision occurs, the products may escape from the nucleus or initiate secondary collisions. Typically, an intranuclear cascade develops. When none of the cascade particles can escape the nucleus, it is assumed that their energies become distributed among all of the nucleons in the nucleus.

Following an intranuclear cascade, the residual nucleus is very likely to be in a highly excited state. In general, subsequent emission of nucleons, alpha particles, and other heavy particles will occur. Detailed descriptions of these particles are determined by Monte Carlo methods in subroutine WEK, which is a modified version of Dresner's program EVAP (1961). The calculations are based on the nuclear evaporation model of Weisskopf (1937), which assumes the nucleus to be in a compound state. In the model of Weisskopf, the energy stored in a compound nucleus can be compared with the heat energy of a solid body or a liquid, and the expulsion of particles is thermodynamically analogous to evaporation from macroscopic bodies. The probability per unit time for the emission of particle j with kinetic energy within dE of E is

$$p_j(E)dE = \gamma_j \, E \, \sigma_{rev}(E)[W_f/W_i]dE \qquad \text{II-2}$$

Here $\gamma_j = g_j \, m_j/\pi^2 \, h^3$, with g_j and m_j the number of spin states and the mass of particle j, respectively, $\sigma_{rev}(E)$ is the cross section for the inverse reaction, and W_f and W_i are the energy level densities of the final and initial nuclei at their respective excitation energies. Equation II-2 is derived

starting with the reciprocity theorem for nuclear reactions (Blatt and Weisskopf, 1937), which states that the probability for a transition proceeding one way in time is equal to the probability for the same transition but with the sense of time reversed. An important assumption in making a meaningful interpretation of Equation II-2 is that the energy-level densities form a continuum of states. This condition is most nearly satisfied for heavy nuclei and for excitations that are large compared to the lowest excitation energy of the nucleus.

The probabilities P_j for emission of the various particles are obtained by integrating $p_j(E)$ over the emitted particle energy. In the calculations, when an emitted particle j is selected, the kinetic energy is sampled from $p_j(E)$. After emission, the probabilities P_j are calculated for the new nucleus and the sampling procedure is repeated. The evaporation continues until the nuclear excitation is reduced to the point where subsequent particle emission is not energetically possible.

An evaporation spectrum falls off very rapidly with increasing energy so that nearly all the evaporated particles are produced below the NMT cutoff energy. The high-energy tail is not transported in NMT.

When a struck nucleus, other than hydrogen, is selected in NMT, BERT and WEK together determine a complete description of the products of the reaction. The cascade products are comprised of protons, neutrons, and π^+, π^-, and π^o mesons. Evaporation products include protons, neutrons, deuterons, tritons, alpha particles, and ^{3}He nuclei. Although descriptions of emitted π^o mesons are made available, these particles are not transported since they decay almost immediately into two very energetic photons.

The relative abundance of nucleon-proton and pion-proton cross-section data has allowed a rather complete description of collisions with hydrogen nuclei. The reactions with hydrogen include nucleon-proton and pion-proton elastic scattering, π^--p charge exchange scattering, nucleon-proton single- and double-pion production, and pion-proton single-pion production.

Pion production from inelastic collisions with hydrogen nuclei is based on the isobar model of Lindenbaum and Sternheimer (1957, 1958, 1961). The calculational scheme is identical to that used in subroutine BERT where pion production may occur within the nucleus. In the calculations, the following compound reaction types for pion creation are considered:

$$N + N \rightarrow N + N^*; \; N^* \rightarrow N + \pi.$$

$$N + N \rightarrow N^* + N^*; \; N^* \rightarrow N + \pi; \; N^* \rightarrow N + \pi.$$

$$\pi + N \rightarrow \pi + N^*; \; N^* \rightarrow N + \pi.$$

Here π and N denote a pion and a nucleon, respectively, and N^* denotes an isobar, that is, an excited nucleon. Implicit in these reactions is the assumption that the initial reaction goes to completion before isobar decay occurs. All isobars are assumed to be defined by a total isotopic spin T of 3/2 and a total angular momentum J of 3/2. Under this assumption, the excited nucleon state is characterized by its mass and z component of isotopic spin T_z. Therefore, isobars may occur having different values of T_z but having the same mass. When an isobar decays, the value of T_z uniquely

determines the available charge states of the decay products. The term "isobar" is thus seen to be appropriate from consideration of the analogous case where nuclei having different charge states but equal mass are called isobars.

At present very little data are available on the isobar angular distributions. In NMT an option is provided whereby the scattering angle of all isobars in the center-of-mass system is selected from one of three distributions: isotropic, directly forward and backward (with equal probability), and 50 per cent isotropic and 50 per cent forward-backward. Isobar decay is assumed to occur isotropically with respect to the isobar at rest.

The Cascade-Evaporation Cutoff Energy

As was mentioned earlier, the nuclear interaction model of intranuclear cascade followed by nuclear evaporation is used to transport particles in NMT down to an arbitrary cutoff energy. Actually there are four cutoff energies corresponding to protons, neutrons, pions, and muons. The cutoff energies for the nucleons are specified by the user and are usually given the same value. Normally the nucleon cutoff is taken to be in the energy range 20-50 MeV since below this energy region the range of charged particles in most materials is very short, and in general the cascade-evaporation model is not applicable.

The cutoff energy for charged pions is calculated in NMT and is equal to the proton cutoff multiplied by the ratio m_π/m_p, where m_π and m_p are the charged pion and proton rest masses, respectively. This procedure arises from the fact that in each medium one table of range versus energy

is used to determine the ranges and inverse ranges (energies) for both protons and charged pions. If $R_p(E_o;E)$ denotes the distance traveled by a proton which, via electronic collisions, has its energy reduced from E_o to $E < E_o$ and $R_\pi(E_o;E)$ denotes the same quantity for charged pions, then the two ranges are related by

$$R_\pi(E_o;E) = \frac{m_\pi}{m_p} R_p\left(\frac{m_p}{m_\pi} E_o; \frac{m_p}{m_\pi} E\right) . \qquad \text{II-3}$$

From this expression, $\frac{m_p}{m_\pi} E$ is the proton cutoff and E is the π cutoff. Thus, if the proton cutoff is input as 50 MeV, the π cutoff is computed to be $\sim$7.4 MeV. A derivation of Equation II-3 is given on page 16. The same scheme is used to calculate ranges and inverse ranges for muons. The muon cutoff is equal to the proton cutoff multiplied by the ratio of the muon rest mass to the proton rest mass.

III. RANGES AND INVERSE RANGES

A charged particle that is heavy compared to an electron will lose energy in electronic collisions when moving through matter. Let $R(E_o;E)$ denote the distance traveled by a heavy particle which, due to electronic collisions only, decelerates from E_o to E. It is assumed in NMT that

$$R(E_o;E) = \int_{E_o}^{E} \langle dT/ds \rangle^{-1} \, dT , \qquad \text{II-4}$$

where $-dT/ds$ is the energy loss to electrons per unit path length, and the brackets denote the expected value. The expected energy loss per unit path length is calculated from

$$-\langle dT/ds \rangle = \frac{4\pi z^2 e^4}{m_e c^2 \beta^2} \left\{ \log_e \left[\frac{2 m_e c^2 \beta^2}{(1-\beta^2) I} \right] - \beta^2 \right\} \sum_{i=1}^{n} N_i Z_i \ , \qquad \text{II-5}$$

where

z = the charge of the particle in units of e,

e = electron charge in electrostatic units,

m_e = electron mass in grams,

c = the speed of light in vacuum in centimeters per second,

β = the particle speed relative to the medium in units of c,

N_i = the density of nuclide type i in units of atoms per cubic centimeter,

Z_i = the charge of nuclide type i in units of e,

$$\log_e I = \sum_{i=1}^{n} N_i Z_i \log_e I_i \Big/ \sum_{i=1}^{n} N_i Z_i \ ,$$

I_i = mean excitation energy of the ith nuclide type,

n = the number of nuclide types in the medium.

This expression for $\langle dT/ds \rangle$ is a simplification of that found in Barkas and Berger (1964).

In NMT energy values E_i are tabulated in increments of equal lethargy starting from the proton energy cutoff ELOP and extending to C × EMAX. EMAX is the maximum energy for particles appearing in the calculation, and C is a scale factor which depends on whether the calculation is to transport nucleons and pions or to transport muons. For each medium, the tabulated values of $R_p(E_i;\text{ELOP})$, where the p denotes proton range, and those of E_i are used in the transport calculation to compute a) the range

to ELOP given E_i, and b) the energy (inverse range) corresponding to a residual range.

Using Equation II-3, ranges and inverse ranges for pions are computed from the proton values. This equation is derived as follows: Starting with Equation II-4, one may write

$$R_p(m_pE_o/m_\pi;m_pE/m_\pi) = \int_{m_pE/m_\pi}^{m_pE_o/m_\pi} S_p^{-1}(T)\, dT ,$$

where $S(T) \equiv -\langle dT/ds \rangle$ and the subscripts p and π denote protons and pions, respectively. Using $T' = m_\pi T/m_p$, the above integral transforms to

$$\frac{m_p}{m_\pi} \int_E^{E_o} S_p^{-1}(m_pT'/m_\pi)\, dT' .$$

From Equation II-5, it may be seen that for a fixed speed v the value of $-\langle dT/ds \rangle$ is the same for particles of different mass provided the particles have the same charge z. If m_pT'/m_π is the kinetic energy of a proton of speed v, the kinetic energy of a pion moving at the same speed is T'. Thus

$$S_p(m_pT'/m_\pi) = S_\pi(T')$$

and

$$R_p(m_pE_o/m_\pi;m_pE/m_\pi) = \frac{m_p}{m_\pi} \int_E^{E_o} S_\pi^{-1}(T')\, dT' = \frac{m_p}{m_\pi} R_\pi(E_o;E) .$$

The ranges and inverse ranges for muons are obtained in the same manner as for pions.

IV. PSEUDO EVENTS AND NUCLEAR DECAY

In section III of this chapter it was mentioned that particle flight trajectories in NMT are sampled from a distribution function which has the form:

$$F_{k,m}(S;E_o) = \int_o^S {}_k\Sigma_m[E(s;E_o)]\, e^{-\int_o^s {}_k\Sigma_m[E(s';E_o)]\, ds'}\, ds \ , \ 0 \leq S \ , \qquad \text{II-6}$$

where the variable definitions are given on page 7, and the subscripts on E have been dropped for brevity. A general outline of the procedure used to obtain sample trajectories from $F_{k,m}(S;E_o)$ is as follows:

1. Let T denote a sample flight trajectory and let M denote a fixed upper bound on ${}_k\Sigma_m[E(s;E_o)]$. Assign i the value 1 and z_o the value 0.
2. Sample x_i from $\int_o^X M\, e^{-Mx}\, dx \ , \ 0 \leq X$.
3. Sample r_i from $\int_o^R dr \ , \ 0 \leq R \leq 1$.
4. Calculate $z_i = z_{i-1} + x_i$.
5. If $r_i \leq {}_k\Sigma_m[E(z_i;E_o)]/M$, assign T the value z_i and stop; otherwise, increment i by 1 and proceed to step 2.

An exposition on this procedure is given in a separate paper (Coleman, 1968). What will be given here is a description of the most important suboperations used to implement the sampling scheme in NMT, which

is based on the one given above. In particular, the details of executing step 5 will be discussed.

In the code, M depends on the particle type k and the material m in which the particle is moving. It is calculated from

$$M_{k,m} = {}_k\Sigma_D(E_k) + {}_k\Sigma^*_{m,H} + \sum_{n=1}^{L_m} \Sigma^*_{m,n} , \qquad \text{II-7}$$

where protons, neutrons, positive pions, neutral pions, negative pions, positive muons, and negative muons are denoted by k = 0, 1, 2, 3, 4, 5, and 6, respectively. The terms in Equation II-7 are defined as follows:

${}_k\Sigma_D(E)$ ≡ the cross section for nuclear decay in inverse centimeters, nonzero for k = 2, 4, 5, and 6;

E_k ≡ the energy at which ${}_k\Sigma_D(E)$ is a maximum;

${}_k\Sigma^*_{m,H}$ ≡ $N_{m,H} \times {}_k\sigma^*_H$;

$N_{m,H}$ ≡ atom density of hydrogen in medium m;

${}_k\sigma^*_H$ ≡ the maximum value of the total microscopic hydrogen cross section in square centimeters. This value is selected from the energy range specified in the calculation and depends on the incident particle type k;

L_m ≡ the number of nuclides, excluding hydrogen, in medium m;

$\Sigma^*_{m,n}$ ≡ $N_{m,n} \times \sigma^*_n$, n = 1, 2,..., L_m;

$N_{m,n}$ ≡ atom density of the nth nuclide in medium m;

$\sigma_n^* \equiv \pi \times (r_n^*)^2$;

$r_n^* \equiv$ an effective nuclear radius in centimeters for which $\rho_n(r_n^*) = 0.01\ \rho_n(0)$;

$\rho_n(r) \equiv$ the intranuclear proton charge density as determined by Hofstadter (1956).

The procedure used in NMT to perform the equivalent of step 5 in the general flight trajectory scheme may be understood by first noting that

$$M_{k,m} \equiv {}_k\Sigma_D(E_k) + {}_k\Sigma^*_{m,H} + \sum_{n=1}^{L_m} \Sigma^*_{m,n} =$$

$$= {}_k\Sigma_D(E) + {}_k\Sigma_{m,H}(E) + \sum_{n=1}^{L_m} {}_k\Sigma_{m,n}(E) + {}_k\Sigma^p_m(E) =$$

$$= {}_k\Sigma_m(E) + {}_k\Sigma^p_m(E) > {}_k\Sigma_m(E) \ ,$$

where, for brevity,

$$E = E(z_i; E_o) \ ,$$

and

${}_k\Sigma^*_{m,H} \geq {}_k\Sigma_{m,H}(E) \equiv$ the total hydrogen cross section at energy E in inverse centimeters,

$\Sigma^*_{m,n} > {}_k\Sigma_{m,n}(E) \equiv$ the nonelastic cross section for the nth nuclide in inverse centimeters,

${}_k\Sigma^p_m(E) \equiv M_{k,m} - {}_k\Sigma_m(E)$.

According to the general sampling scheme on page 17, the last step must be satisfied with probability ${}_k\Sigma_m(E)/M_{k,m}$ and dissatisfied with probability $1 - {}_k\Sigma_m(E)/M_{k,m} = {}_k\Sigma^p_m(E)/M_{k,m}$. For this reason, ${}_k\Sigma^p_m(E)$ is often regarded as the total cross section for an apparent or pseudo nuclear event. Pseudo cross sections for nuclear decay and for nuclear interaction with the various nuclides are defined as follows:

$$ {}_k\Sigma^p_D(E) \equiv {}_k\Sigma_D(E_k) - {}_k\Sigma_D(E) \ , $$

$$ {}_k\Sigma^p_{m,H}(E) \equiv {}_k\Sigma^*_{m,H} - {}_k\Sigma_{m,H}(E) \ , $$

$$ {}_k\Sigma^p_{m,n}(E) \equiv \Sigma^*_{m,n} - {}_k\Sigma_{m,n}(E) \ , \quad n = 1, 2, \ldots, L_m \ . $$

The code first selects an event from the probability distribution

$$ \frac{{}_k\Sigma^p_D(E)}{M'_{k,m}(E)} \ , \ \frac{{}_k\Sigma^*_{m,H}}{M'_{k,m}(E)} \ , \ \frac{{}_k\Sigma^*_{m,1}}{M'_{k,m}(E)} \ , \ldots , \ \frac{{}_k\Sigma^*_{m,L_m}}{M'_{k,m}(E)} \ , \qquad \text{II-8} $$

where

$$ M'_{k,m}(E) \equiv M_{k,m} - {}_k\Sigma_D(E) \ . $$

These probabilities sum to 1. They correspond, respectively, to a pseudo decay event, a tentative collision with hydrogen, and tentative collisions with nuclides 1 through L_m. The possible outcomes in this selection do not include "real" nuclear decay. Decay is accounted for by multiplying the particle statistical weight by the nondecay probability $M'_{k,m}(E)/M_{k,m}$. It is important to note that the statistical weight is modified unconditionally, regardless of the selection that is made from Equation II-8.

If a tentative collision with hydrogen is selected, then a real collision is selected with conditional probability ${}_k\Sigma_{m,H}(E)/{}_k\Sigma^*_{m,H}$ and a pseudo collision is selected with conditional probability $1 - {}_k\Sigma_{m,H}(E)/{}_k\Sigma^*_{m,H} = {}_k\Sigma^p_{m,H}(E)/{}_k\Sigma^*_{m,H}$. For hydrogen, a real or pseudo collision is selected using an explicit value for the total hydrogen cross section ${}_k\Sigma_{m,H}(E)$. When a tentative collision with nuclide n has occurred, the particle is tracked within a hypothetical nucleus using the intranuclear cascade subroutine BERT. With probability ${}_k\Sigma_{m,n}(E)/\Sigma^*_{m,n}$, a nuclear interaction will occur, and with probability $1 - {}_k\Sigma_{m,n}(E)/\Sigma^*_{m,n}$, the incident particle will pass through the nucleus uncollided. However, an explicit value for ${}_k\Sigma_{m,n}(E)$ is not used in determining whether the collision is real or apparent since ${}_k\Sigma_{m,n}(E)$ is not available.

The probabilities for all of the individual "real" events sum to ${}_k\Sigma_m(E)/M'_{k,m}(E)$. For nucleons, $M'_{k,m}(E) = M_{k,m}$, and consequently no statistical weight compensation is necessary. For mesons, $M'_{k,m}(E) \neq M_{k,m}$, and hence the distribution of flight trajectories will differ from that given in Equation II-6. However, the statistical weight modification mentioned on page 19 is such that unbiased estimates can be obtained for any quantities that depend on the distribution of meson flight trajectories. Examples of such quantities are pion flux and the muon source arising from pion decay.

The code could have been programmed to include "real" meson decay, in which case no statistical weight compensation would be necessary. The primary intention of prohibiting "real" meson decay is to improve estimates of the muon source that results from pion decay.

V. ASSUMPTIONS ON THE FATE OF PIONS BELOW THE CUTOFF ENERGY IN NMT

The π^+ mesons appearing below the cutoff energy in NMT are assumed to decay immediately into μ^+ mesons. A low-energy π^- meson may decay or be absorbed into a nucleus. The absorption cross section depends on the material atom density, whereas the cross section for decay is independent of atom density. When the atom density is $\sim 10^{21}$-10^{22}, which is the case for most materials, absorption will be far more probable than decay. The converse will be true for π^- mesons moving through a very rare material such as the upper atmosphere of the earth. Accordingly, an option is offered in NMT as to the treatment of all π^- mesons appearing below the cutoff energy. When absorption is selected, all π^- mesons appearing below the cutoff energy are forced to interact via the intranuclear-cascade routine. If decay is specified, all π^- mesons appearing below the cutoff energy are assumed to decay immediately into μ^- mesons.

CHAPTER III

DESCRIPTION OF THE CALCULATIONS

All of the calculations were performed with the target and moderator being described as coaxial cylinders. The geometry used is illustrated in Figure 1, page 3. In most cases, the dimensions were as given in this figure with the exceptions to be noted.

Incident protons were assumed to pass along the axis of symmetry, through a cylindrical void, and into the target. The axial position was defined as positive to the target side of the vacuum-target interface. The radial position of protons entering the void was sampled from a two-dimensional Gaussian distribution having a variance of four centimeters. This description of the radial spread of the incident beam was based on photographs from the experiments of Fraser et al. (1965). Small-angle deflections of primary protons due to Coulomb interactions with nuclei were calculated using the description given by Rossi (1965). With the possible exception of target heating as a function of position, most of the results are relatively insensitive to the incident proton beam spread and the multiple Coulomb scattering.

A cutoff energy of 25 MeV was used in NMT. Negative pions reaching their energy cutoff were assumed to undergo nuclear interaction via Bertini's intranuclear-cascade code. For the calculations with a heavy water moderator, a very important blanket assumption was made concerning nuclear collisions with deuterium above 25 MeV. Since NMT cannot treat

collisions with deuterium by any means other than the intranuclear-cascade model, all macroscopic cross-section data for deuterium, including the energy and angle description of secondaries, were assumed to be identical to the same data for hydrogen. In defense of this approximation, it is pointed out that the population of all particle types above 25 MeV is small in the moderator, and hence the contribution to the thermal-neutron flux by collisions in the moderator above 25 MeV is very small.

Neutrons appearing below 25 MeV were transported in 05R down to 0.5 eV. In 05R, nonelastic collisions with O, Sn, Pb, and U were described using compound nucleus formation followed by nuclear evaporation. Nonelastic reactions with D and Be were assumed to be entirely (n,2n). The momentum distribution of neutrons produced from the n(d,2n)p reaction was calculated using the scheme suggested by Kalos, Goldstein, and Ray (1962), in which it is assumed that the momenta of secondaries is uniformly distributed in the center-of-mass system. Neutrons produced from the (n,2n) reaction with Be were assumed to be emitted isotropically in the laboratory system. The energy spectra of these neutrons were obtained from the data of Buckingham, Parker, and Pendlebury (1961). Table I gives the cross-section reference data for all of the 05R calculations.

To obtain the thermal-neutron flux as a function of position, the density of neutrons appearing in the system below 0.5 eV was averaged over each of 312 cylindrical volume annuli. The resulting averaged data were used as the thermal-neutron source in a single-energy-group flux

TABLE I

REFERENCES FOR CROSS-SECTION DATA USED IN O5R CALCULATIONS

Element or Nuclide	
H	Irving and Gillen (1966).
D	Kalos, Goldstein, and Ray (1962).
Be	Buckingham, Parker, and Pendlebury (1961), Doherty (1965), Joanou (1964), and Zabel (1957).
O	Hughes and Harvey (1958).
Sn	Hughes and Harvey (1958).
Pb	Hughes and Harvey (1958) and Bertin et al. (1964).
^{235}U	Hughes and Harvey (1958) and Bertin et al. (1964).
^{238}U	Hughes and Harvey (1958), Bertin et al. (1964), and Webster (1966).

calculation using EXTERMINATOR-2 (Fowler et al., 1967), a two-dimensional diffusion code. Diffusion theory calculations of the thermal-neutron flux in water were compared with Monte Carlo estimates of the same quantity using several source distributions. The results were in good agreement.

Figure 3 illustrates the average thermal-neutron source between z = 30 cm and z = 37.5 cm as a function of radial position for 1500-MeV protons incident on a Pb target in a water moderator. The numbers above the histogram in Figure 3 are calculated estimates of the relative standard error expressed in per cent. These error estimates are typical of those obtained for the thermal-neutron source in all of the calculations.

In the uranium-target calculations, the amount of ^{235}U present was assumed to be 0.22 per cent, in agreement with that used in the experiments of Fraser et al. (1965). If no thermal fissioning occurred, neutrons reaching thermal would diffuse and ultimately be lost through leakage or absorption. Coupling of the slowing-down calculation using 05R with the thermal diffusion calculation using EXTERMINATOR-2 would be straightforward in this case. However, some thermal fissioning was present in the uranium target, requiring a neutron-transport calculation which was cyclic in energy. Such a calculation using both codes, 05R and EXTERMINATOR-2, would have been very impractical. Instead, the uranium-target calculations below 25 MeV were performed using only 05R. All neutrons below 0.5 eV were transported using 0.025-eV cross sections and assuming isotropic scattering in the laboratory system. The thermal flux was deduced from the collision density in each of 312 cylindrical volume annuli.

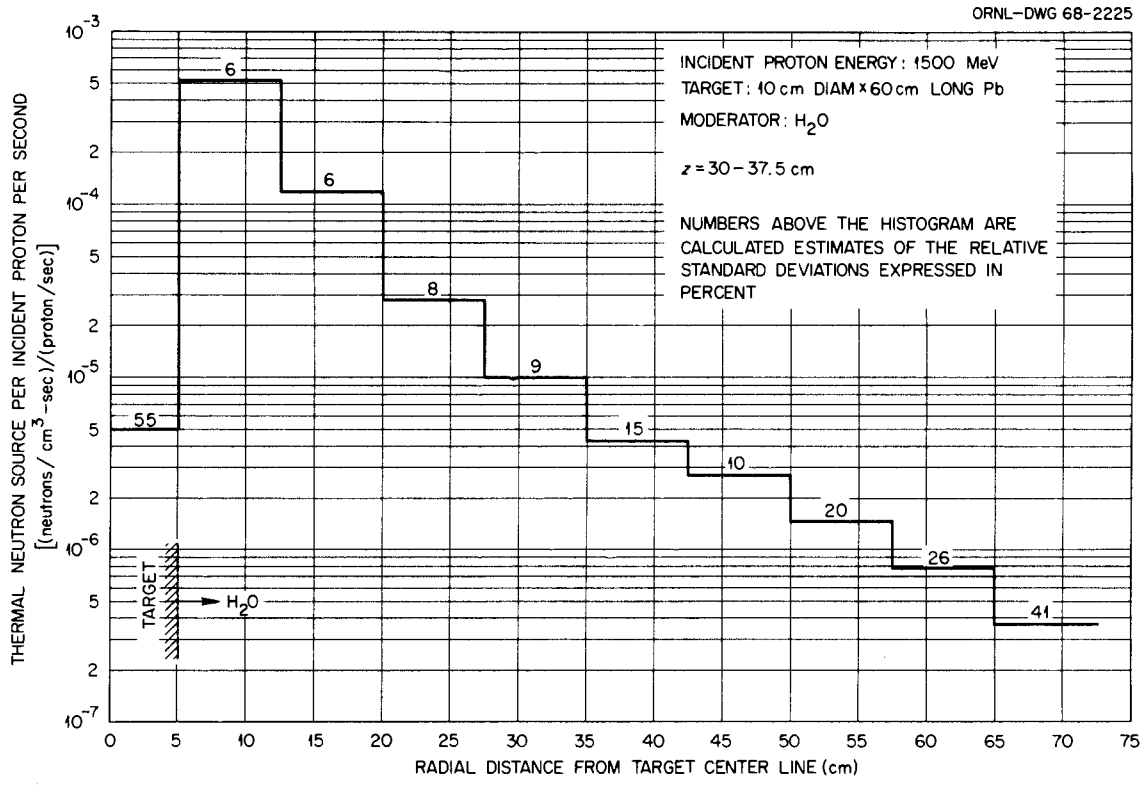

Figure 3. Average thermal-neutron source per incident proton per second between z = 30 cm and z = 37.5 cm as a function of radial position for 1500-MeV protons incident on a Pb target in an H_2O moderator.

In NMT, the calculations of heat-producing energy release in the target and moderator accounted separately for (a) ionization losses by all charged particles, other than muons, and the kinetic energy of all recoiling nuclei, (b) residual excitation of nuclei following nuclear evaporation, (c) π° meson production, and (d) ionization losses by muons. In 05R, neutrons below 25 MeV undergo nuclear collisions in which heat-producing energy is released via protons, alpha particles, nuclear excitation, and nuclear recoil. This energy, along with the gamma-ray energy from thermal-neutron captures, was calculated in the target and moderator. The data on energy released as a function of position in the target include only the energy released through the processes mentioned in (a). This approximation should be adequate for targets other than uranium since 90 to 95 per cent of the total energy released in the target is due to the processes mentioned in (a). In a uranium target, much of the energy released is due to fissioning, and this energy is not included in the data on energy released as a function of position in the target. A spatial map of fission heat in the target would have been a special case, requiring additional provisions within the 05R code that were not necessary for other target materials. The calculated values for total energy released in the target do include energy from fissioning below 25 MeV. For both ^{235}U and ^{238}U, an average value of 178 MeV per fission (Glasstone and Edlund, 1952) was assumed at all energies in 05R.

CHAPTER IV

RESULTS, COMPARISON WITH EXPERIMENT, AND DISCUSSION

I. THERMAL-NEUTRON-FLUX DISTRIBUTIONS

Figures 4 through 14 illustrate the calculated radial distribution of the thermal-neutron flux for various combinations of incident proton energy, target material, and moderator material. In each of these figures, radial distributions are given for two fixed axial positions z, and in each figure one of the two z values was selected corresponding to where the maximum flux occurred. The experimental data of Fraser et al. (1965) are given in each of these figures for comparison with the calculated results. With one exception, all of the data were calculated using the dimensions given in Figure 1, page 3. The Be target used by Fraser et al. was 4 inches square and 36 inches long. In the calculations, the cylindrical target radius was chosen so that the target volume was equal to that of the experimental target.

Radial flux distributions in an H_2O moderator for 1500-MeV incident protons are given in Figures 4 through 7 for targets of Be, Sn, Pb, and U in that order. For the Pb target, in Figure 6, calculated results are also given for a D_2O moderator.

Figures 8, 9, and 10 correspond to incident proton energies of 540, 750, and 900 MeV. Radial flux distributions for a Pb target in moderators of H_2O and D_2O are given in each of these figures. The comparisons of calculated and experimental data in Figures 4 through 10

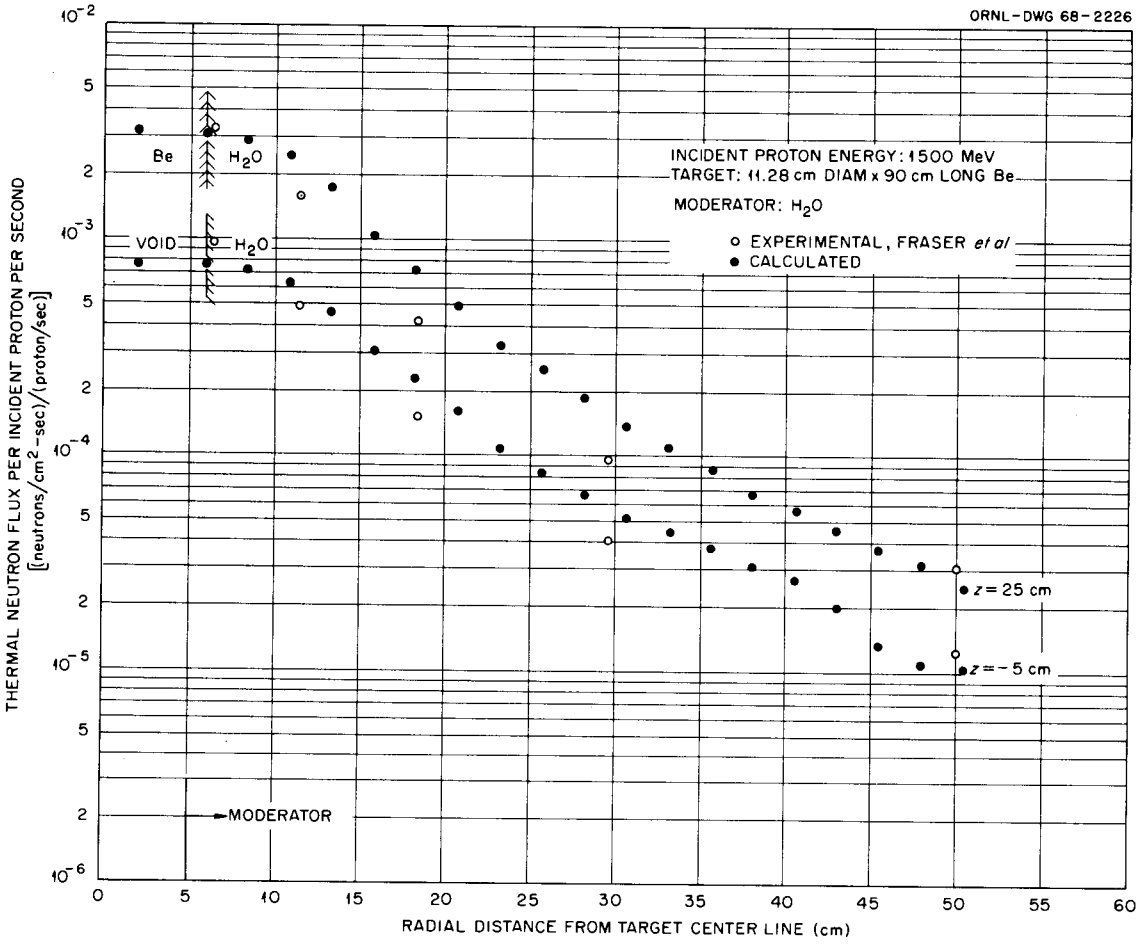

Figure 4. Thermal-neutron flux per incident proton per second as a function of radial position at z = -5 cm and z = 25 cm for 1500-MeV protons incident on a Be target in an H_2O moderator.

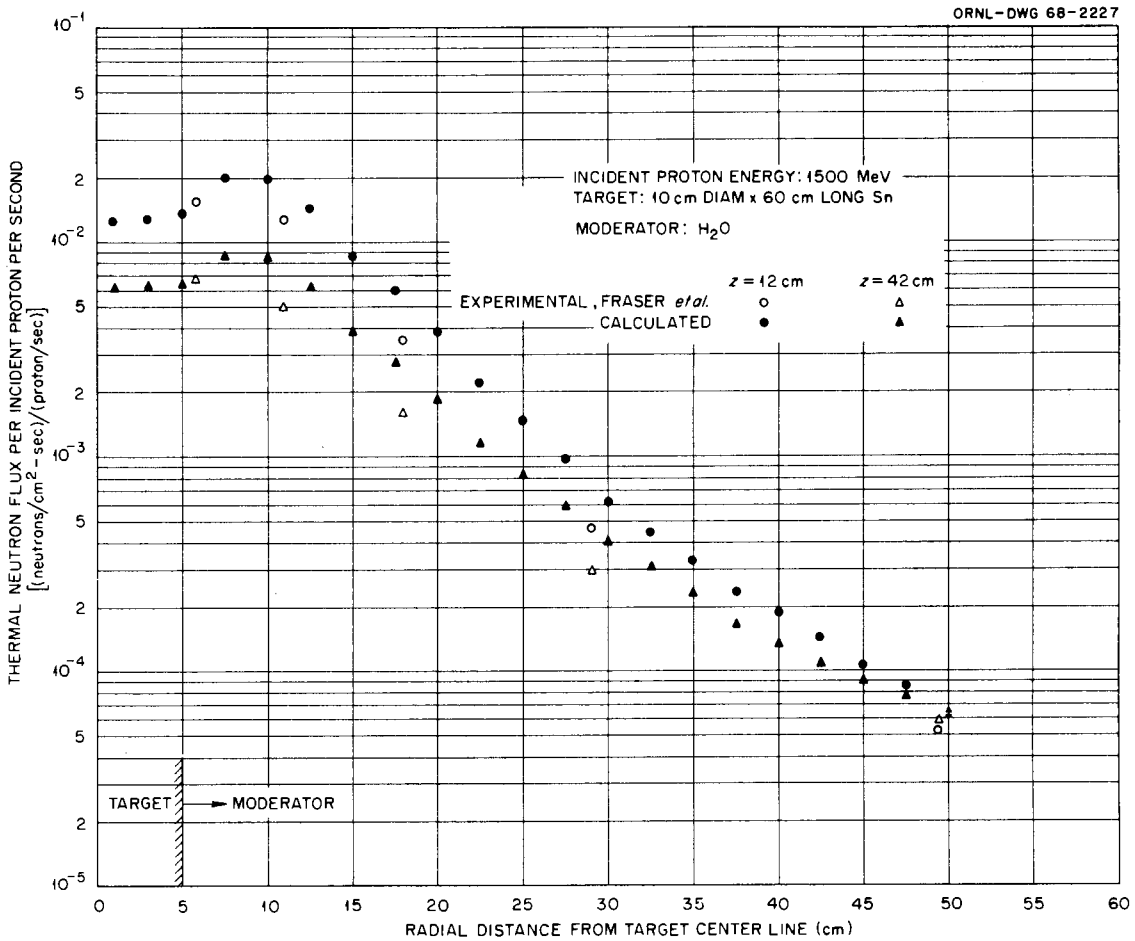

Figure 5. Thermal-neutron flux per incident proton per second as a function of radial position at z = 12 cm and z = 42 cm for 1500-MeV protons incident on an Sn target in an H_2O moderator.

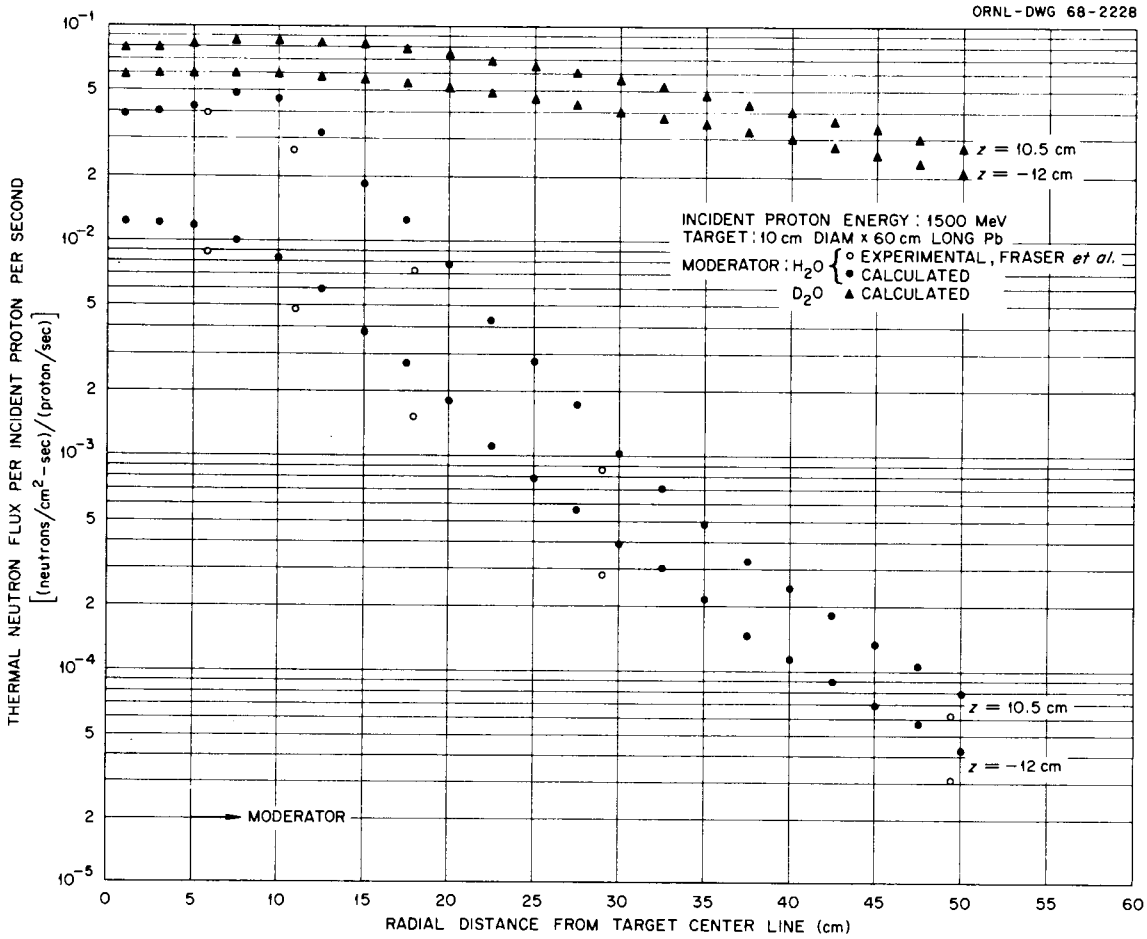

Figure 6. Thermal-neutron flux per incident proton per second as a function of radial position at z = -12 cm and z = 10.5 cm for 1500-MeV protons incident on a Pb target in moderators of H_2O and D_2O.

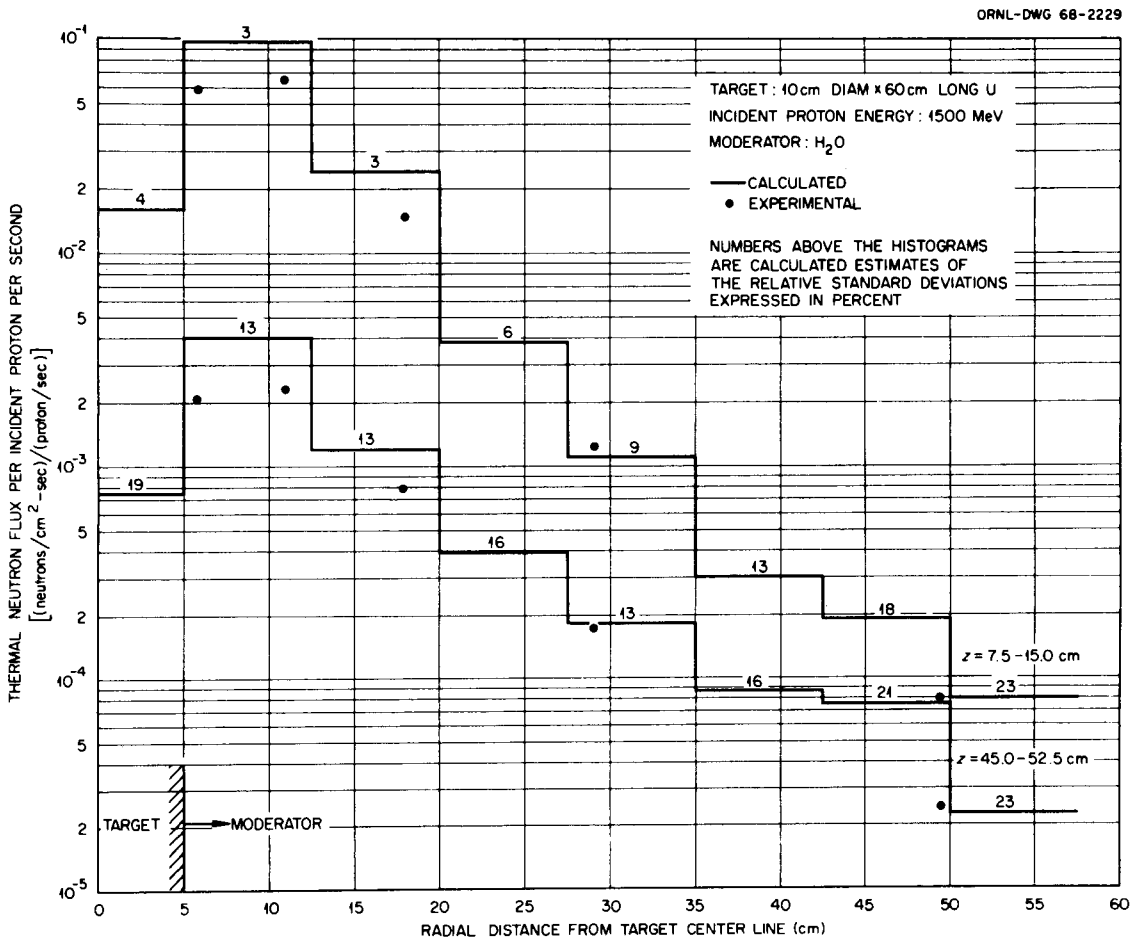

Figure 7. Thermal-neutron flux per incident proton per second as a function of radial position between z intervals 7.5-15 cm and 45-52.5 cm for 1500-MeV protons incident on a U target in an H_2O moderator.

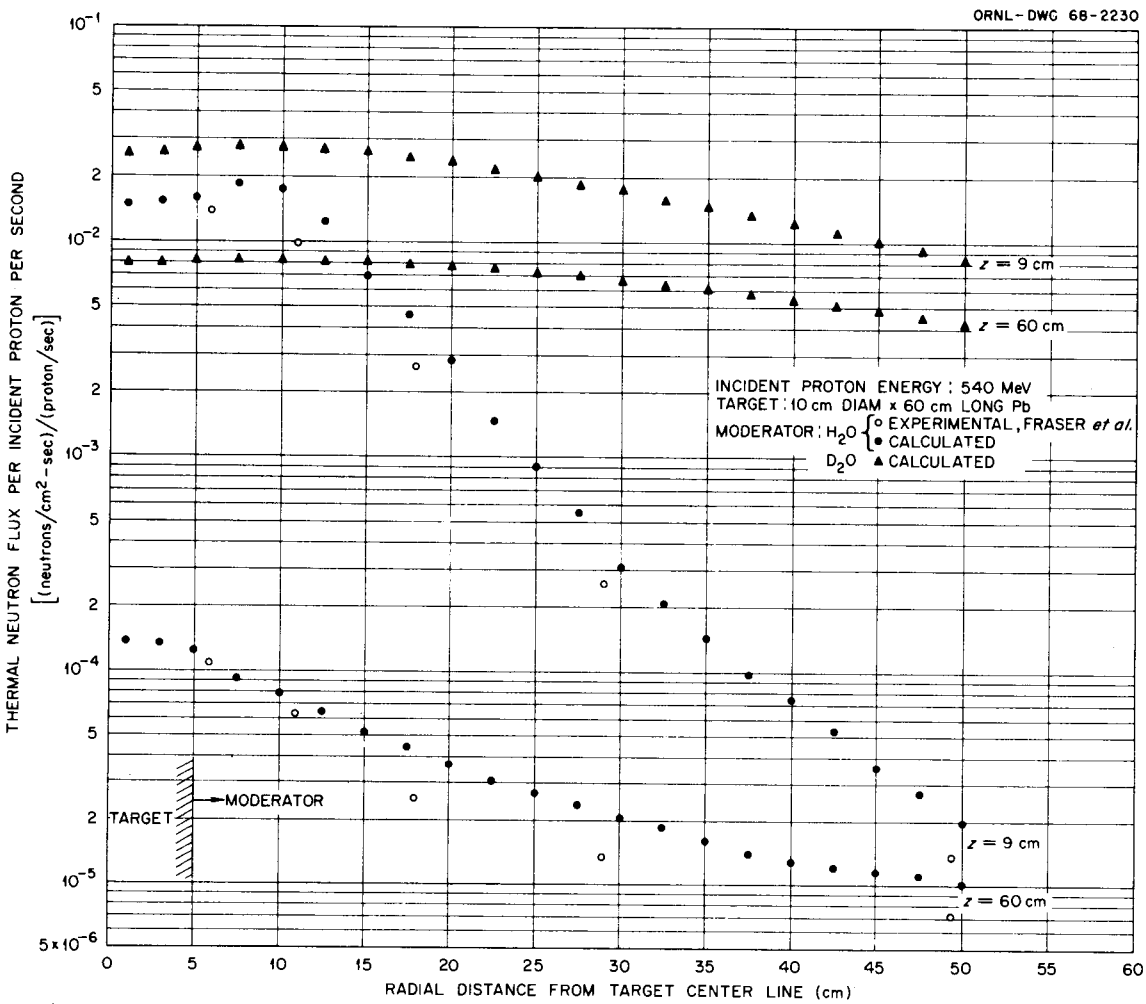

Figure 8. Thermal-neutron flux per incident proton per second as a function of radial position at z = 9 cm and z = 60 cm for 540-MeV protons incident on a Pb target in moderators of H_2O and D_2O.

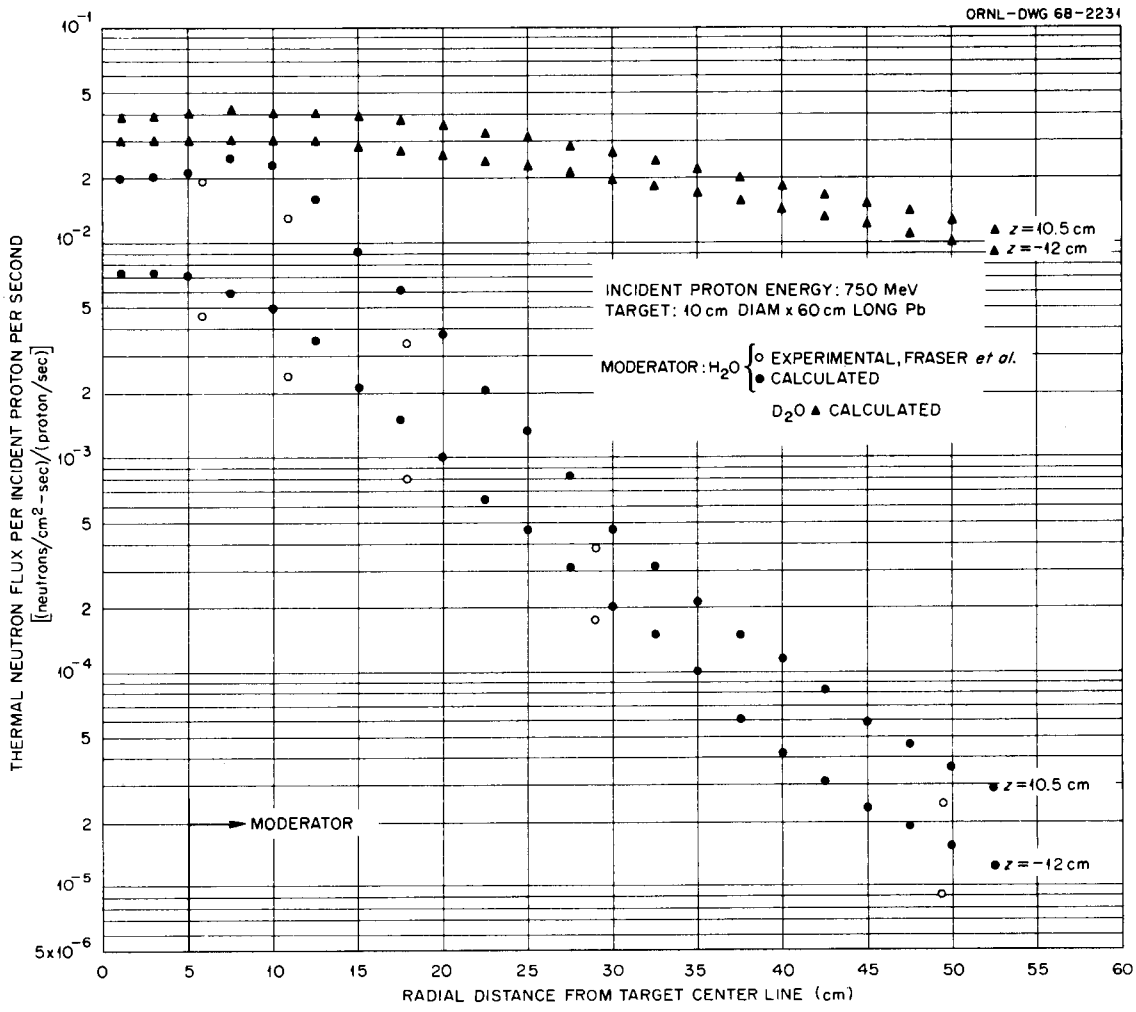

Figure 9. Thermal-neutron flux per incident proton per second as a function of radial position at z = -12 cm and z = 10.5 cm for 750-MeV protons incident on a Pb target in moderators of H_2O and D_2O.

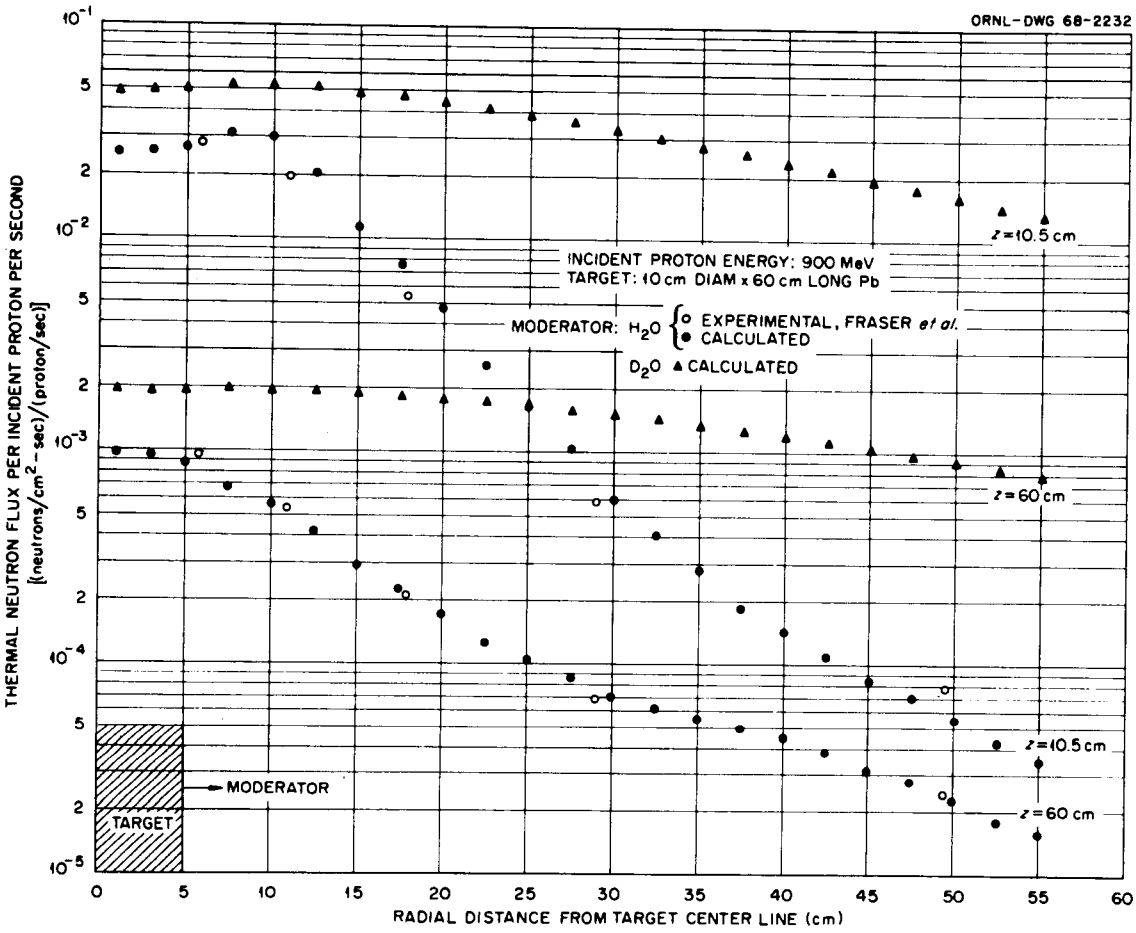

Figure 10. Thermal-neutron flux per incident proton per second as a function of radial position at z = 10.5 cm and z = 60 cm for 900-MeV protons incident on a Pb target in moderators of H_2O and D_2O.

appear to be equally good for all combinations of target material and incident proton energy. According to the Pb target calculations, replacing the H_2O with D_2O increases the maximum flux by a factor of approximately 1.6. However, the more obvious advantage of D_2O is that the flux decreases very slowly with increasing distance from the point of maximum flux. In Figure 10, for z = 10.5 cm, the ratio of the flux in D_2O to the flux in H_2O increases from 1.7 at radial position R = 8 cm to 100 at R = 35 cm.

In Figures 4 through 10 the comparisons of calculated and experimental data are absolute; that is, there has been no renormalization of either experimental or calculated data. Figures 11 through 14 are additional comparisons of calculated and experimental thermal-neutron-flux distributions for various combinations of incident proton energy, target material, and moderator material. However, arbitrary normalizations have been applied to the experimental data in these figures since absolute normalizations were not available.

When an H_2O moderator is used, there is very little thermal-neutron leakage, and one may consider the total number of thermal-neutron captures in the moderator as a figure of merit for target selection. Calculated results for this quantity as a function of incident proton energy for targets of Be, Sn, Pb, and U are given in Figure 15. The calculated relative standard error for each of these data was less than 5 per cent. Direct comparisons with the neutron-production data of Fraser et al. cannot be made since their data are corrected to include

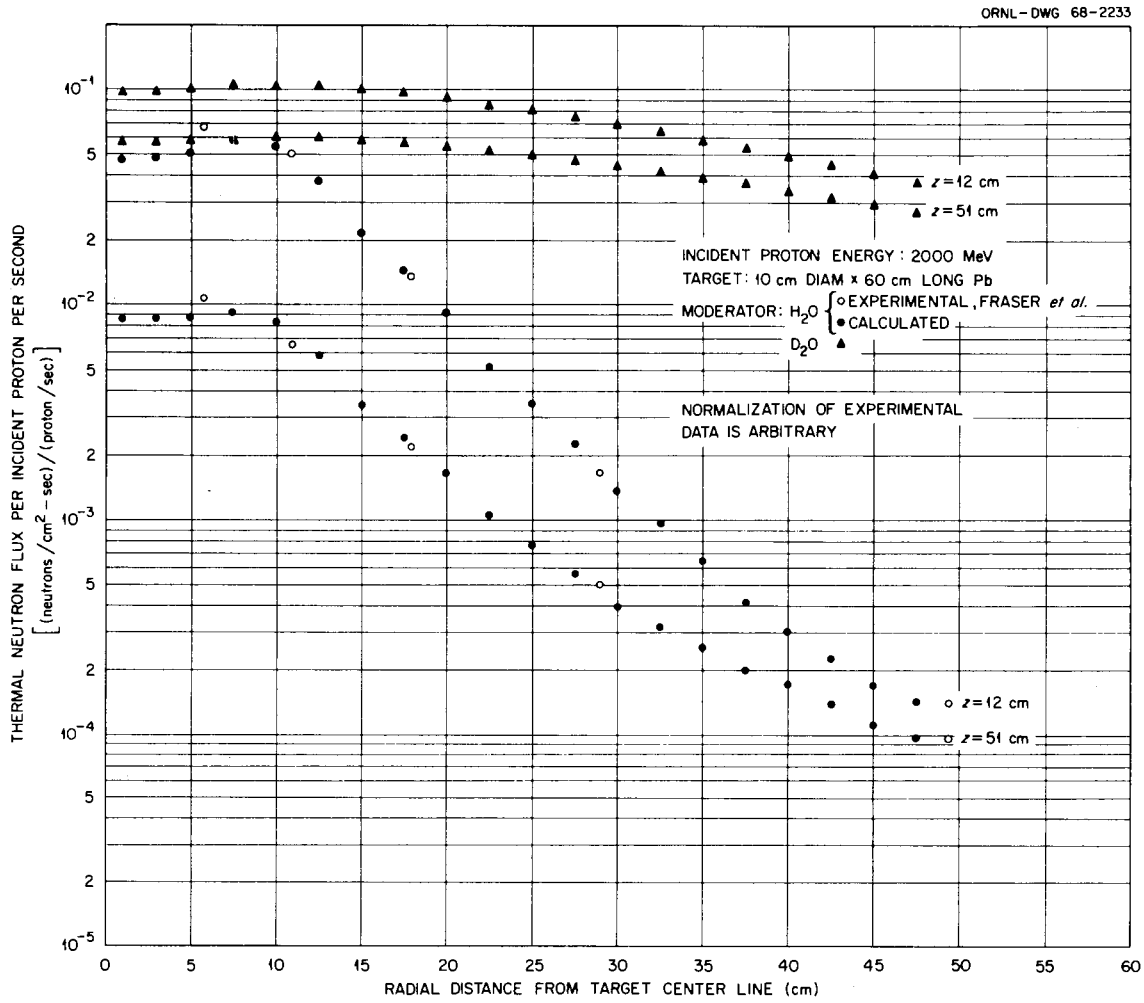

Figure 11. Thermal-neutron flux per incident proton per second as a function of radial position at z = 12 cm and z = 51 cm for 2000-MeV protons incident on a Pb target in moderators of H_2O and D_2O.

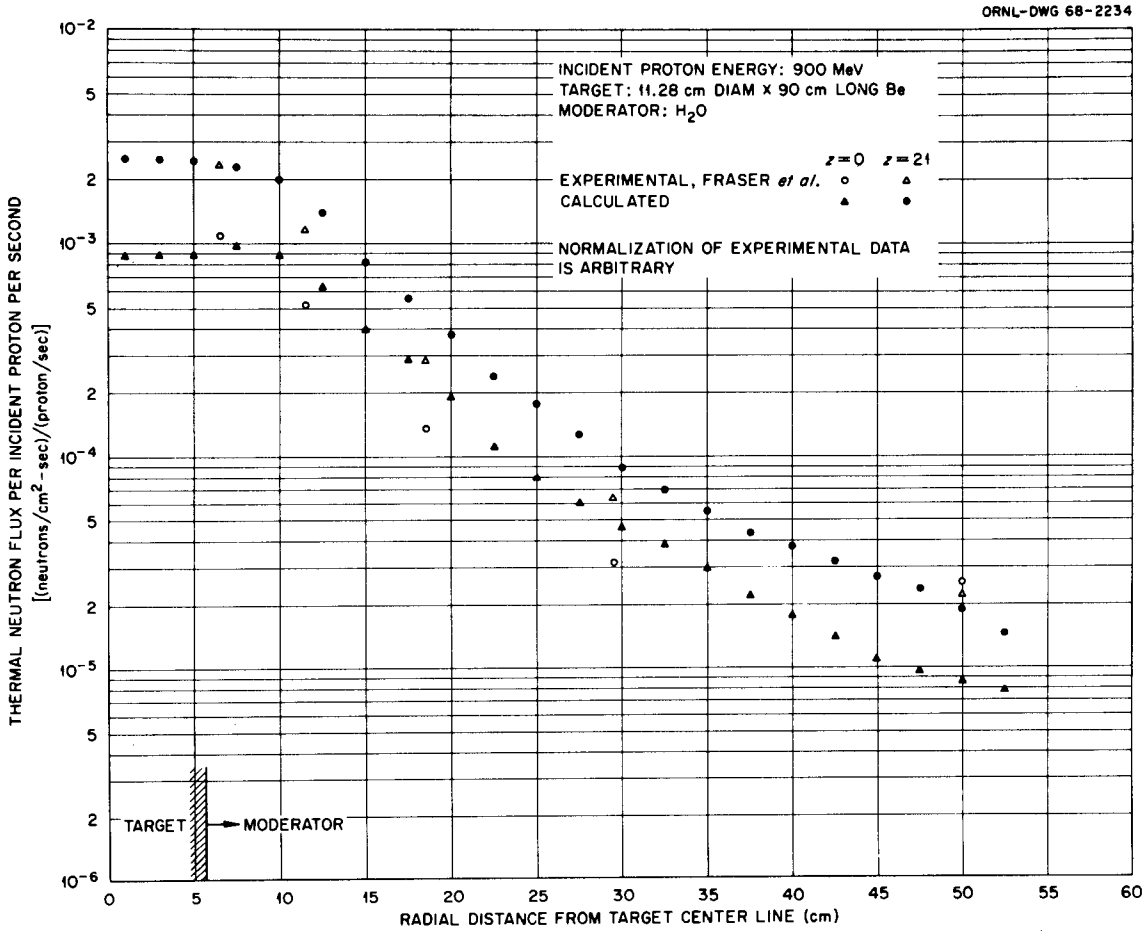

Figure 12. Thermal-neutron flux per incident proton per second as a function of radial position at z = 0 cm and z = 21 cm for 900-MeV protons incident on a Be target in an H_2O moderator.

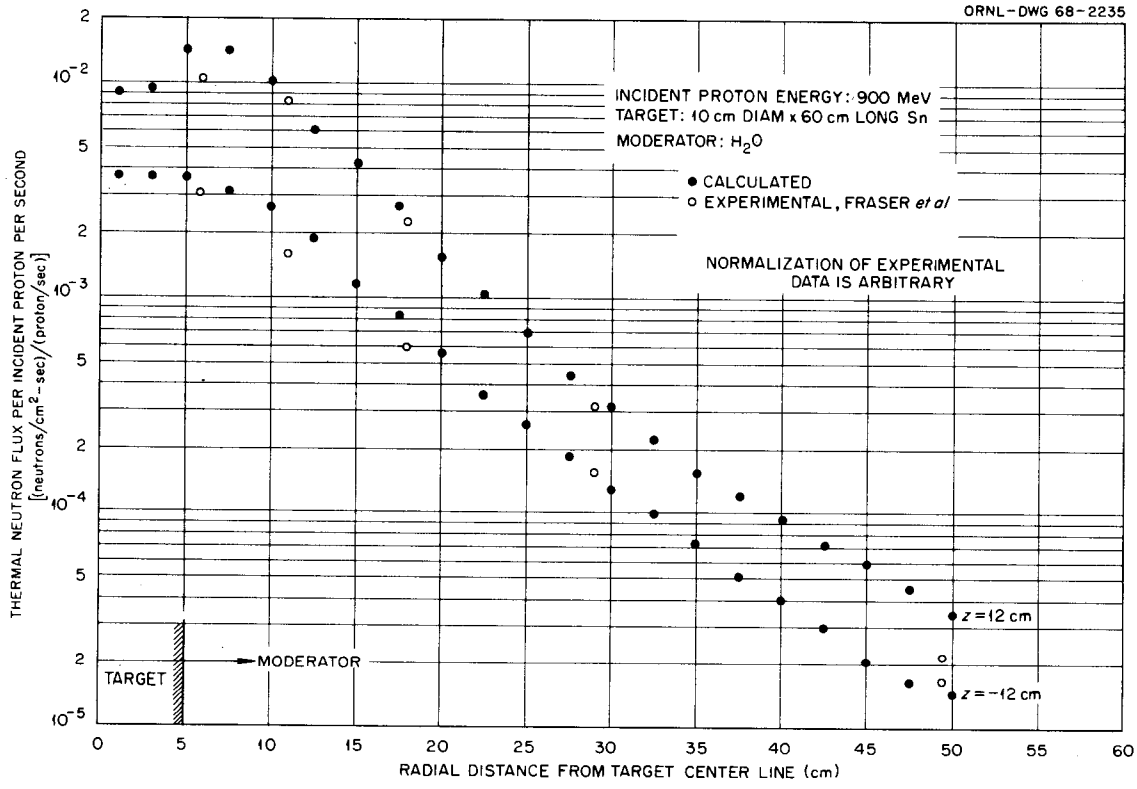

Figure 13. Thermal-neutron flux per incident proton per second as a function of radial position at z = -12 cm and z = 12 cm for 900-MeV protons incident on an Sn target in an H_2O moderator.

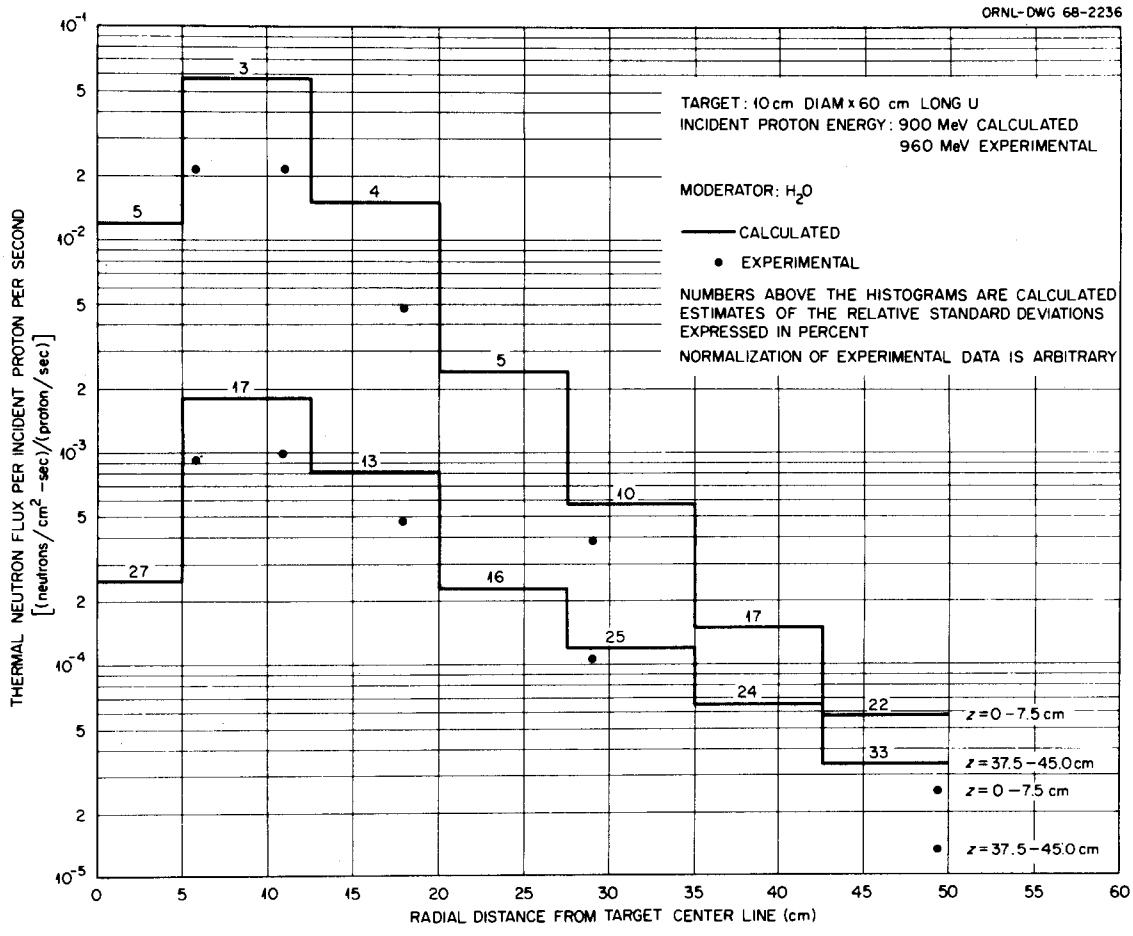

Figure 14. Thermal-neutron flux per incident proton per second as a function of radial position between z intervals 0-7.5 cm and 37.5-45 cm for 900-MeV protons incident on a U target in an H_2O moderator.

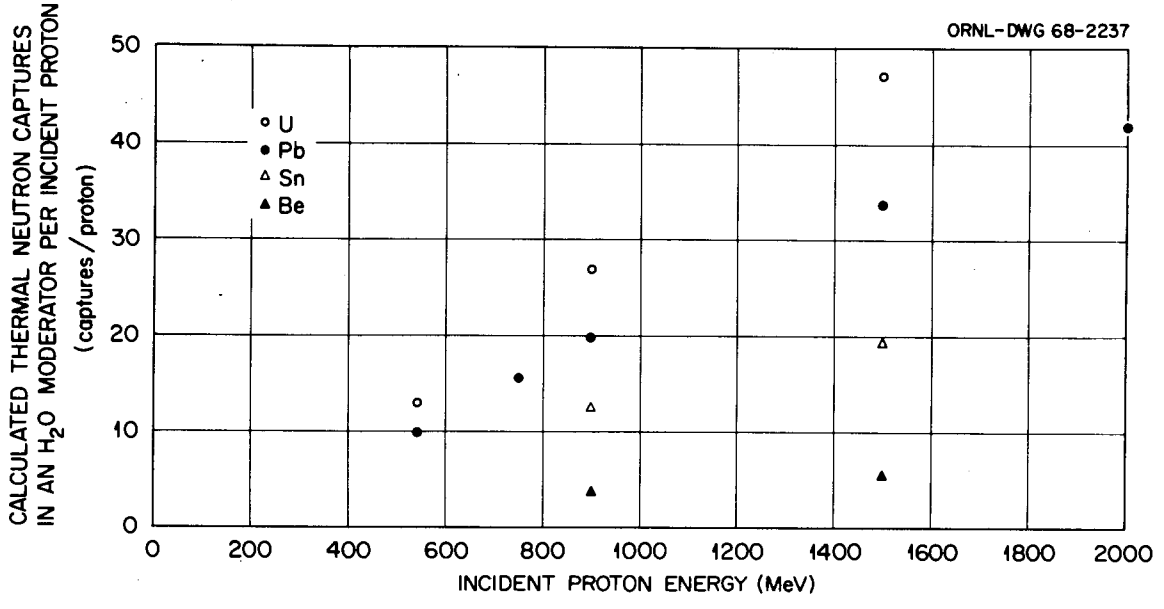

Figure 15. Calculated thermal-neutron captures in an H_2O moderator per incident proton as a function of incident proton energy for various target materials.

captures occurring in the target. When a D_2O moderator is used, very few of the neutrons which are thermalized are captured in the D_2O. It follows that thermal-neutron capture is not a criterion for target selection when a bare D_2O moderator is used.

The maximum thermal-neutron flux, which was obtained from the data in Figures 4 through 10, pages 30 through 36, and Figures 11 through 14, pages 38 through 41, is plotted as a function of incident proton energy in Figure 16. These data, while perhaps being more significant than the data for thermal-neutron capture, do not fully reveal the advantage of a D_2O moderator. In particular, for moderators of H_2O and D_2O no information is given which compares the rate at which the flux decreases with increasing distance from the point of maximum flux.

II. HEAT PRODUCTION

In this section results are given for the production of energy that is eventually transferred as heat. For brevity, such energy will be referred to as heat energy. The processes that account for this energy are cited in Chapter III, page 28, and in Table II.

In Table II results are given at three incident proton energies for the heat energy produced in the target and moderator, using a Pb target and the geometry illustrated in Figure 1, page 3. The data are broken down according to the individual processes responsible for the total heat-energy release.

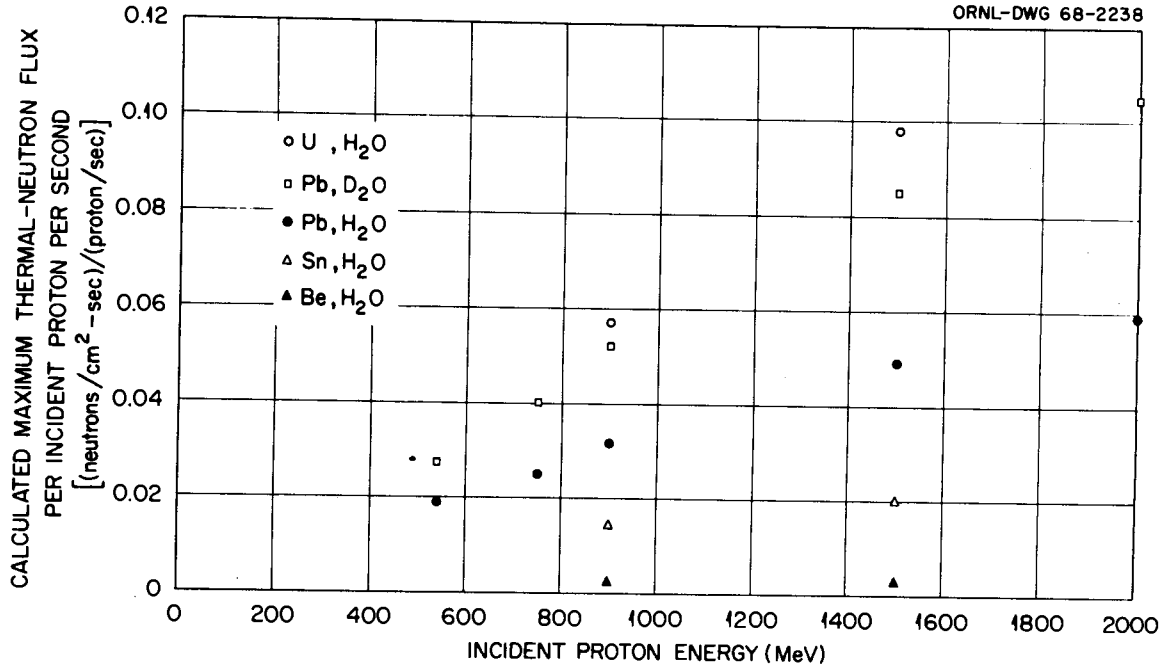

Figure 16. Calculated maximum thermal-neutron flux per incident proton per second as a function of incident proton energy for various target materials.

TABLE II

HEAT-PRODUCING ENERGY RELEASE IN AN ING USING A Pb TARGET AT THREE VALUES OF INCIDENT PROTON ENERGY E_o

Process Type*	Heat-Energy Release (MeV/Incident Proton)					
	E_o = 540 MeV		E_o = 900 MeV		E_o = 2000 MeV	
	Target	Moderator	Target	Moderator	Target	Moderator
a	331.40	46.4	388.40	115.70	543.30	264.60
b	4.80	2.8	8.10	6.80	13.72	18.09
c	0.96	∿0	8.40	1.08	46.25	11.41
d	0.11	∿0	0.63	0.17	1.30	1.16
e	7.03 (9.62)	76.3 (56.38)	15.46 (20.78)	158.9 (118.9)	36.15 (47.30)	378.33 (290.41)
Total	344.3 (346.9)	125.5 (105.6)	421.0 (426.3)	282.8 (242.6)	640.7 (651.9)	673.6 (585.7)

*Process type definitions:

a. The ionization loss by charged particles other than muons excluding that mentioned in e, and the kinetic energy from nuclear recoil excluding that mentioned in e.

b. Nuclear excitation excluding that mentioned in e.

c. The kinetic energy of π^o mesons.

d. The ionization losses by muons.

e. For nuclear interactions below 25 MeV, the energy from protons, alpha particles, nuclear excitation, nuclear recoil, and the gamma-ray energy produced from thermal-neutron capture.

In Table II the moderator material has not been specified since calculations using H_2O and then D_2O produced essentially no change in any of the heat-energy data except for the gamma-ray energy produced from thermal-neutron capture, which is included in process type e. Where different values were obtained using a D_2O moderator, these numbers are given in parentheses. The data are broken down similarly in Table III, which gives heat energy released in the target and in an H_2O moderator for 900-MeV protons incident on targets of Be, Sn, and U. The relative standard error for the data in Tables II and III range from approximately 2 per cent for process-type-a data in the target to 25 per cent for some values corresponding to process type d.

The data in Tables II and III do not account for all of the incident proton energy. Particle leakage from the system, the binding energy required in the nuclear interactions, and meson rest energy account for the remainder of the incident proton energy. From Table II it may be seen that 2000-MeV protons incident on a Pb target in an H_2O moderator release 640.7 MeV in the target and 673.6 MeV in the moderator for a total of 1314 MeV per incident proton. Using the calculated value of 43 neutrons released per incident proton and 7 MeV as the average binding energy of a bound neutron, one can account for approximately 300 MeV as neutron binding energy. The calculations show that neutron leakage accounted for 187 MeV and charged-particle leakage accounted for 105 MeV. Thus, about 1900 MeV of the incident-particle energy is accounted for. In addition to this, there is some energy which goes into binding energy when charged particles are produced by

TABLE III

HEAT-PRODUCING ENERGY RELEASE IN AN ING USING TARGETS OF Be, Sn, AND U FOR 900-MeV INCIDENT PROTONS

Process Type*	Heat-Energy Release (MeV/Incident Proton)					
	Be		Sn		U	
	Target	H_2O	Target	H_2O	Target	H_2O
a	245.80	244.70	355.10	169.20	421.40	80.50
b	12.34	7.38	8.33	8.50	8.38	5.62
c	21.20	2.61	7.66	0.85	8.94	0.10
d	0.48	1.21	0.61	0.32	0.51	0.14
e	1.90	48.49	14.50	125.80	856.00†	123.50
Total	281.72	304.39	386.20	304.67	1295.23	209.86

*The process types are defined in the footnote to Table II.

†This value includes the energy release from fissioning.

nuclear interaction and some energy which goes into rest energy of mesons, so roughly, at least, an energy balance is obtained in this case. Similar considerations in the other cases always enable one to obtain a reasonable energy balance.

Data on the total heat energy released in the target as a function of incident proton energy for various target materials are given in Figure 17. The dimensions of the target and moderator are as noted previously.

The maximum neutron-flux data in Figure 16, page 44, together with the data on heat-energy production in Figure 17, should be very useful in selecting the target material for a potential ING. If it is desired to maintain a fixed maximum flux with a fixed proton-beam energy, a larger value of the maximum neutron flux Φ_{max} per incident proton will decrease the required beam current, and hence reduce the cost associated with maintaining the required beam current. At the same time, a smaller value of H, the heat-energy release in the target per incident proton, will reduce the cost associated with the removal of heat.

Heat-energy production as a function of position in a Pb target for three different incident proton energies is given in Figure 18. The data are presented as radial plots for the six axial increments indicated. Radial and axial increments were selected with the intent of obtaining a uniform distribution in statistical error. The calculated relative standard error averaged approximately 7 per cent with the largest single deviation being 30 per cent.

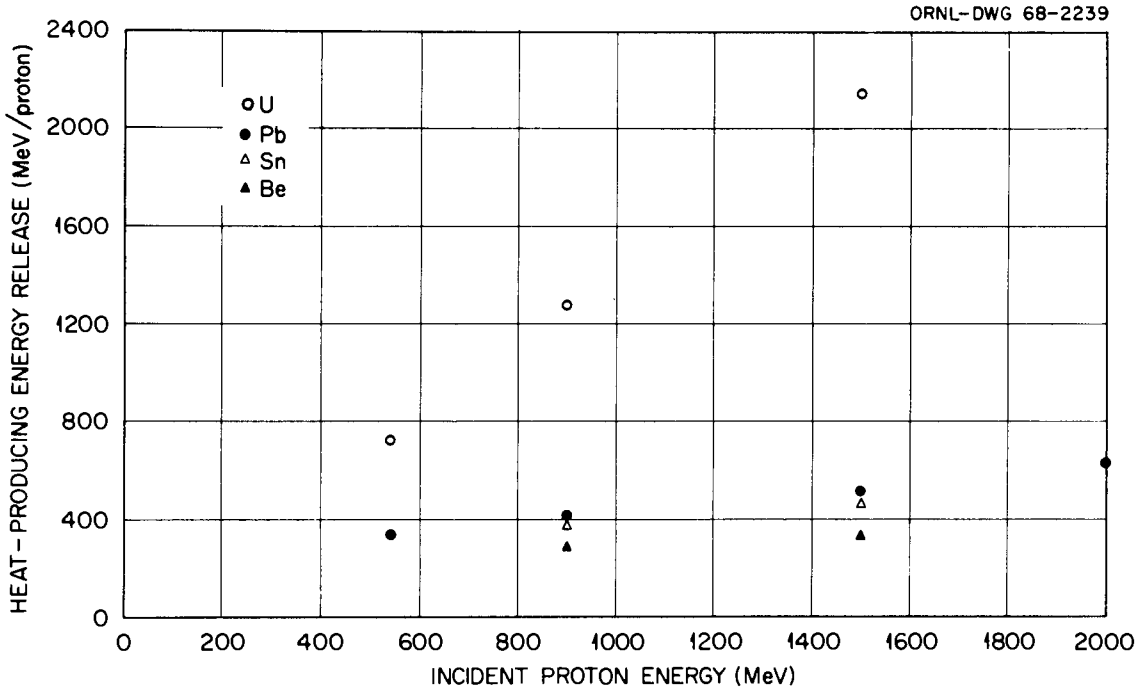

Figure 17. Heat-producing energy release per incident proton as a function of incident proton energy for various target materials.

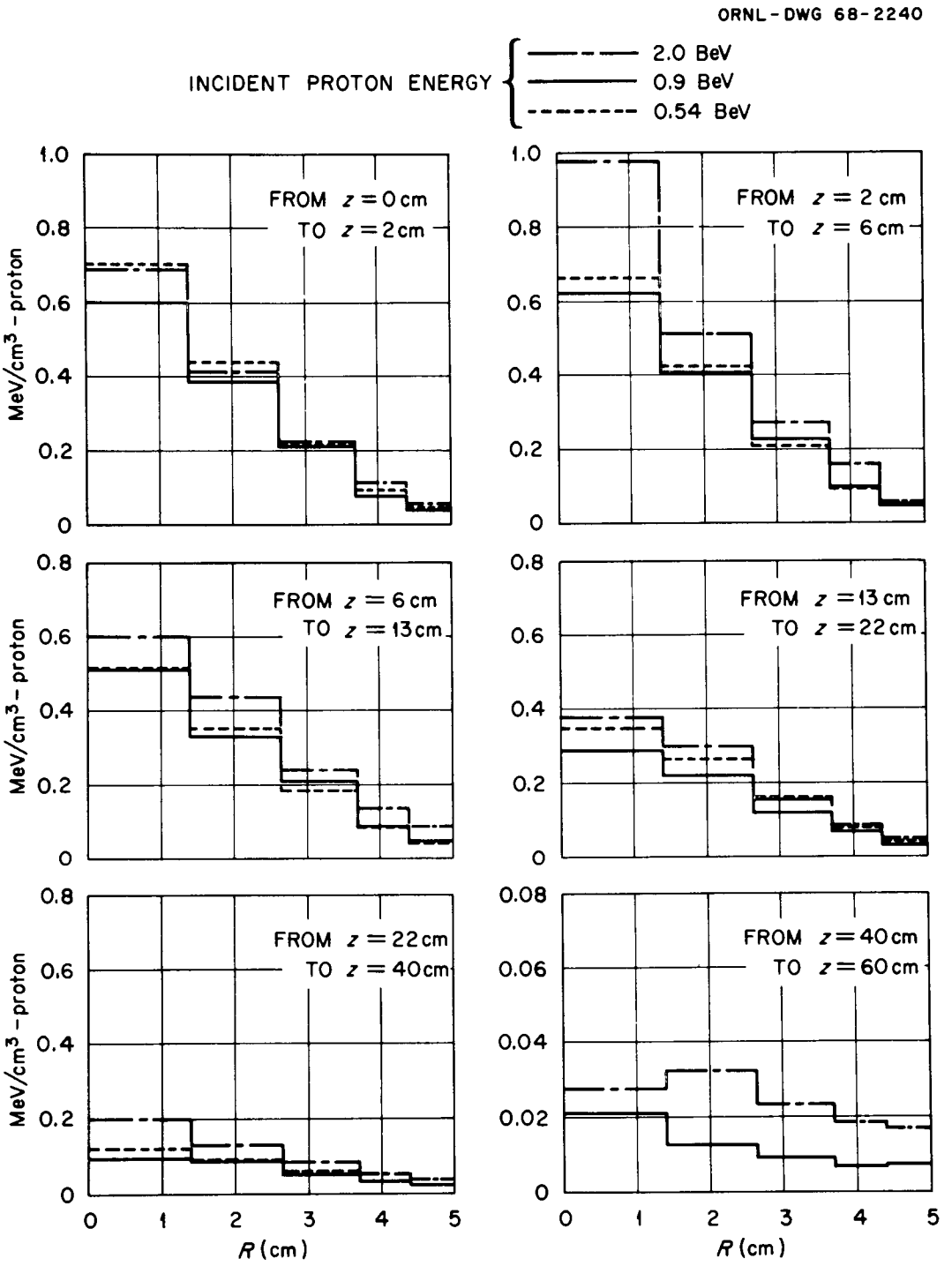

Figure 18. Heat-producing energy release per unit volume per incident proton as a function of radial position R in a Pb target for 6 axial increments and 3 incident proton energies. Target dimensions: 10-cm diameter by 60 cm long.

In Figure 19, heat-energy production is given as a function of position in targets of Be, Sn, and U for an incident proton energy of 900 MeV. The magnitude and behavior of the calculated statistical error were very similar to that obtained for the data in Figure 18.

III. CONCLUSIONS ON TARGET SHAPE

Results on neutron production as a function of position in Pb targets of 5- and 10-cm radii for 900-MeV protons are given in Figure 20. These data do not include a very small fraction of the neutron production which is induced by neutron collisions below 25 MeV, that is, by neutron collisions in the 05R calculation. From this figure, it may be seen that an additional target volume beyond a 5-cm radius does not appreciably affect the spatial distribution of neutron production within the 5-cm radius. The relative standard error for the data in Figure 20 averaged $\sim$10 per cent and ranged to a maximum value of 32 per cent.

The range of 900-MeV protons in Pb is approximately 50 cm. Note that the neutron production is insignificant beyond this distance. This was found to be the case for other combinations of incident proton energy and target material as well.

For the combination of a Pb target and a D_2O moderator, most of the capture in the target occurs in the thermal-energy range. Hence, the relative effectiveness of any region in the target may be judged by the ratio of neutron production to thermal-neutron capture in that region. With a D_2O moderator, the thermal flux is nearly flat in a Pb target. These considerations, together with the neutron-production data in Figure 20, suggest the target shape given in Figure 21. The proposal in

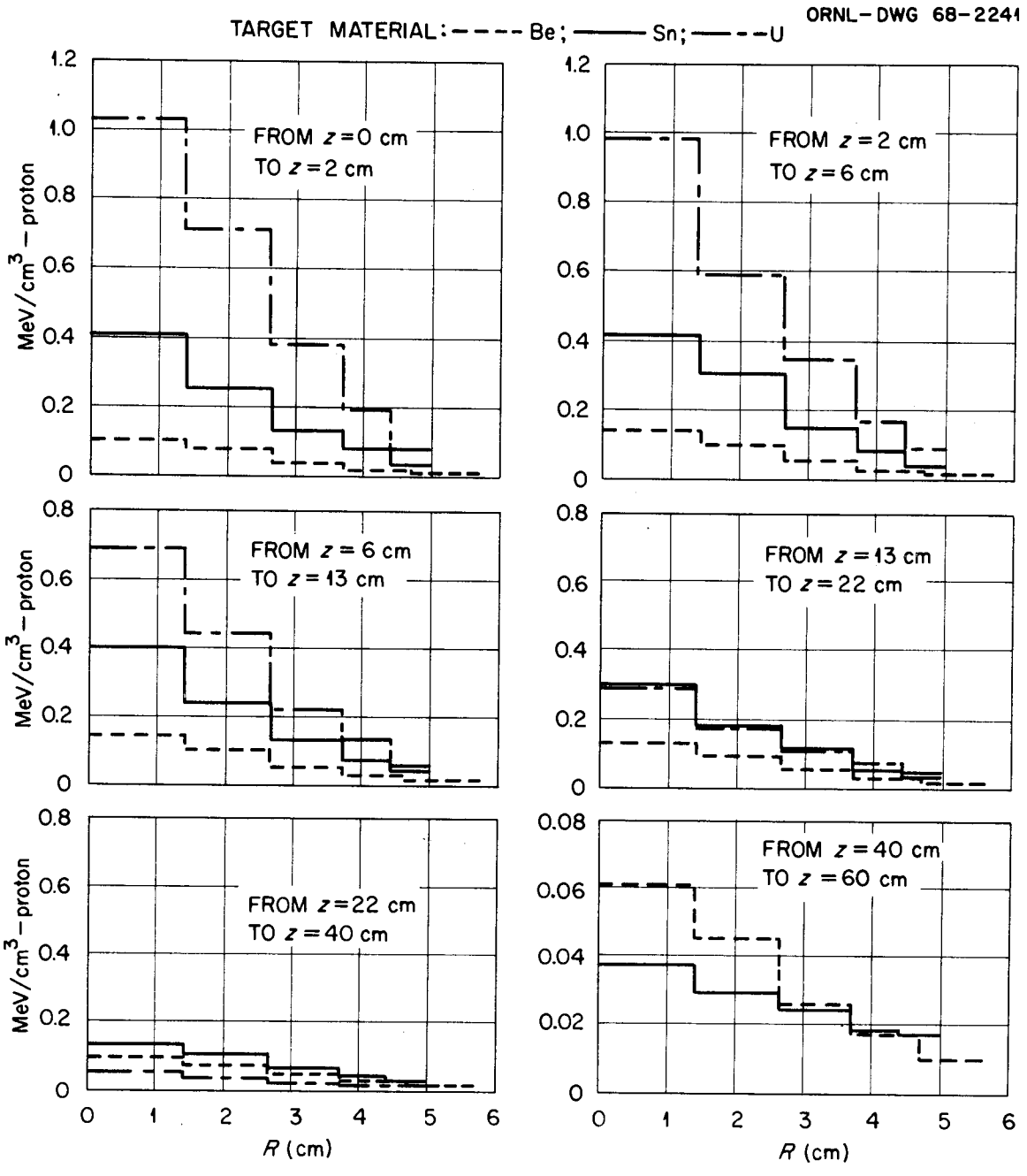

Figure 19. Heat-producing energy release per unit volume per incident proton as a function of radial position R in targets of Be, Sn, and U for 6 axial increments. Incident proton energy: 900 MeV. Target dimensions for Sn and U: 10-cm diameter by 60 cm long. Target dimensions for Be: 11.28-cm diameter by 90 cm long.

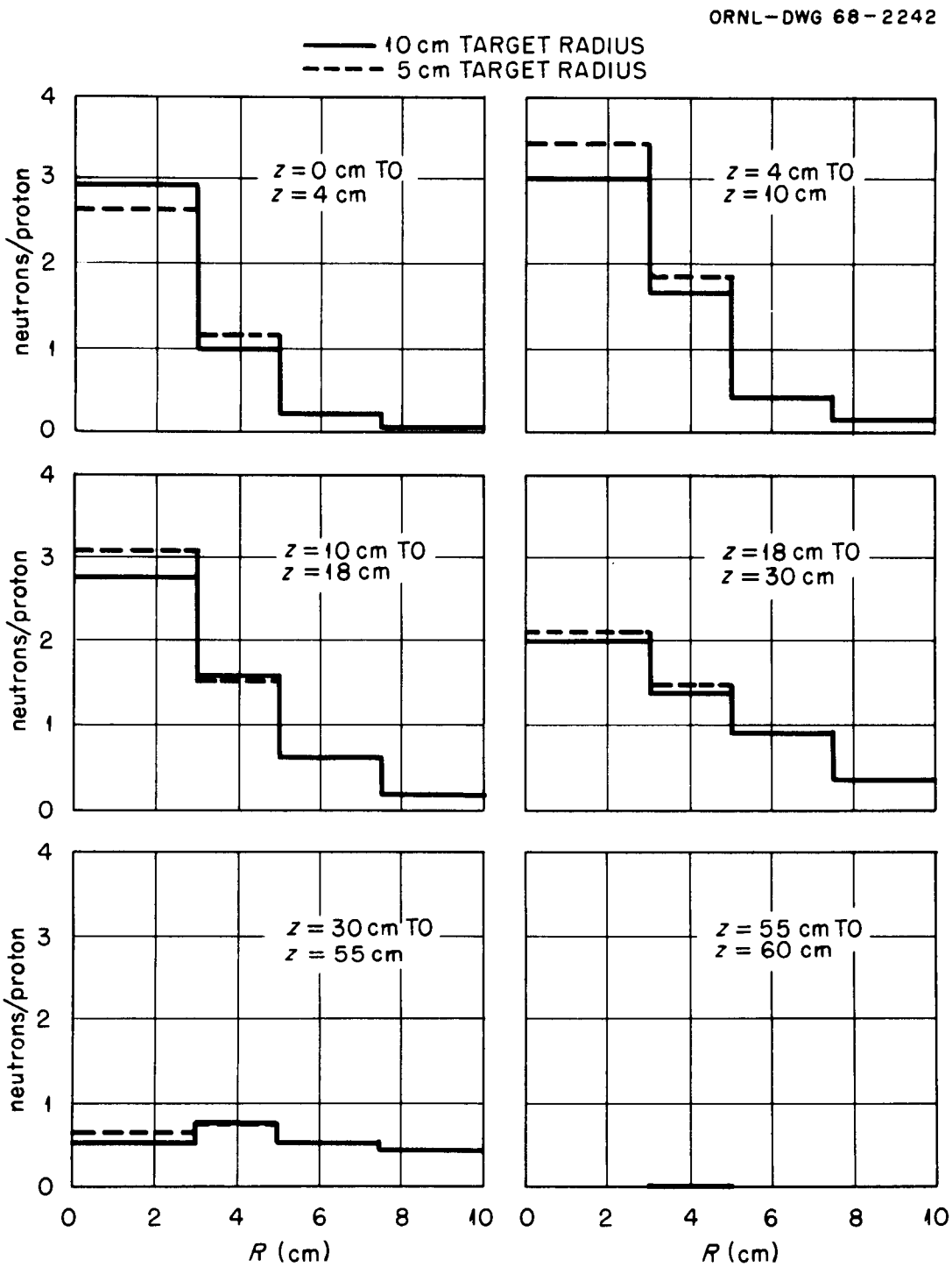

Figure 20. Neutron production per incident proton as a function of radial position R for 6 axial increments using Pb targets of 5- and 10-cm radius. Incident proton energy: 900 MeV.

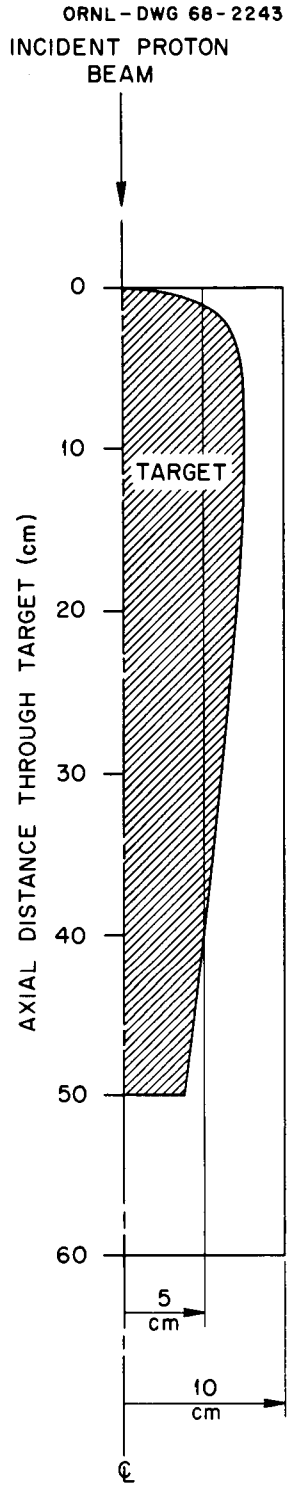

Figure 21. Probable shape for a Pb target using 900-MeV incident protons.

Figure 21 for a maximum target radius of less than 10 cm is based on the data in Figure 22. Here the thermal-neutron flux is plotted as a function of radius for three axial positions using a D_2O moderator and Pb targets of 5- and 10-cm radii. The maximum thermal flux occurs for z = 10 cm. The most important observation to be made from the data in this figure is that for a Pb target in a D_2O moderator the thermal-neutron flux is rather weakly dependent on the target shape, and therefore the precise target shape is probably not very important. Fraser (1965) has considered the use of a liquid lead-bismuth target. The magnitude of the neutron production in Bi is approximately equal to that in an equal volume of Pb whereas Bi has a considerably lower thermal-neutron-capture cross section than Pb. It follows that for a lead-bismuth combination the precise target shape will be even less important than in a Pb target.

IV. SOME CALCULATIONS FOR VARIOUS MODERATOR ARRANGEMENTS

In Figure 23 the calculated radial variation of the thermal-neutron flux is given at z = 10 centimeters for various moderator configurations. A 900-MeV incident proton beam and a 5-cm-radius by 60-cm-long Pb target were used in calculating all of the data. For configuration No. 1 in Figure 23, the geometry is identical to that given in Figure 1, page 3, and the moderator is entirely D_2O. In configuration No. 2, the D_2O moderator has been reduced in radius to 65 centimeters and in length to 150 centimeters. This corresponds to a 61 per cent volume decrease in D_2O. In configuration No. 3 an H_2O reflector has been added to the bare D_2O in configuration No. 2. For configuration No. 1, the integrated thermal-neutron

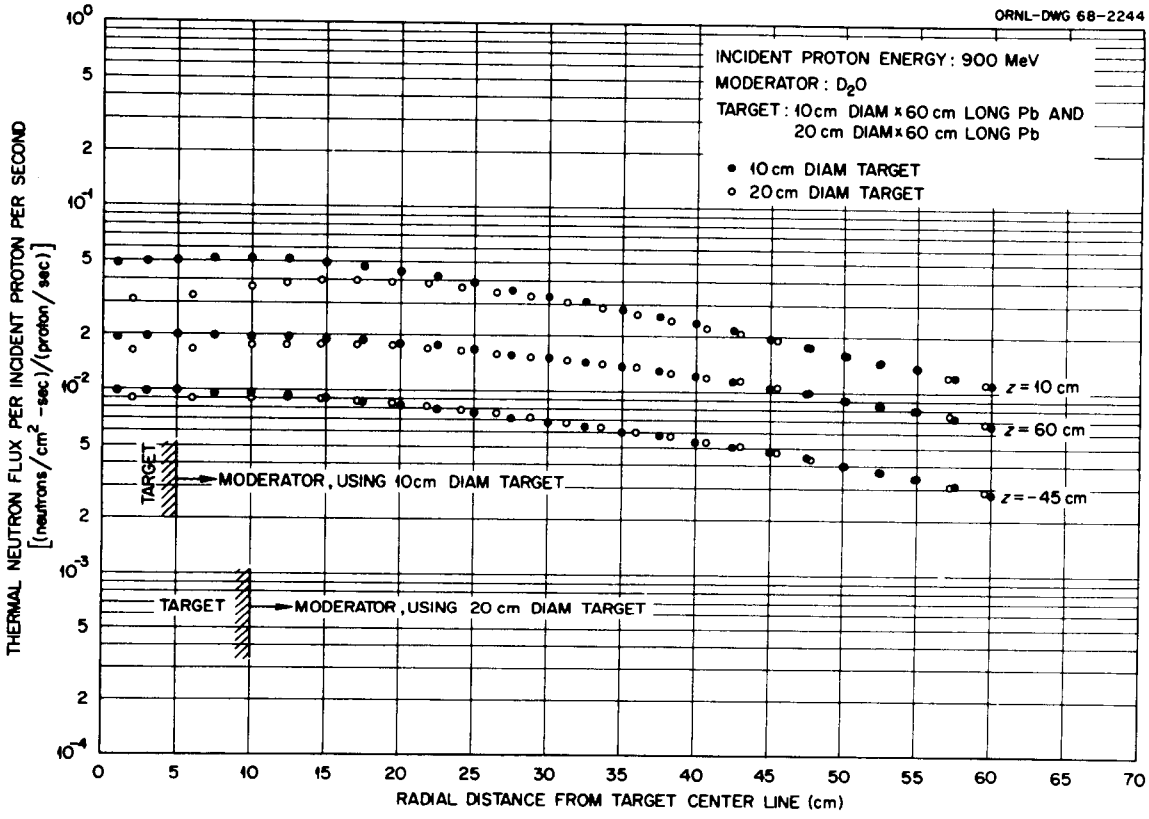

Figure 22. Comparisons of radial thermal-neutron-flux distributions at z = -45, 10, and 60 cm using Pb targets of 5- and 10-cm radius in a D_2O moderator.

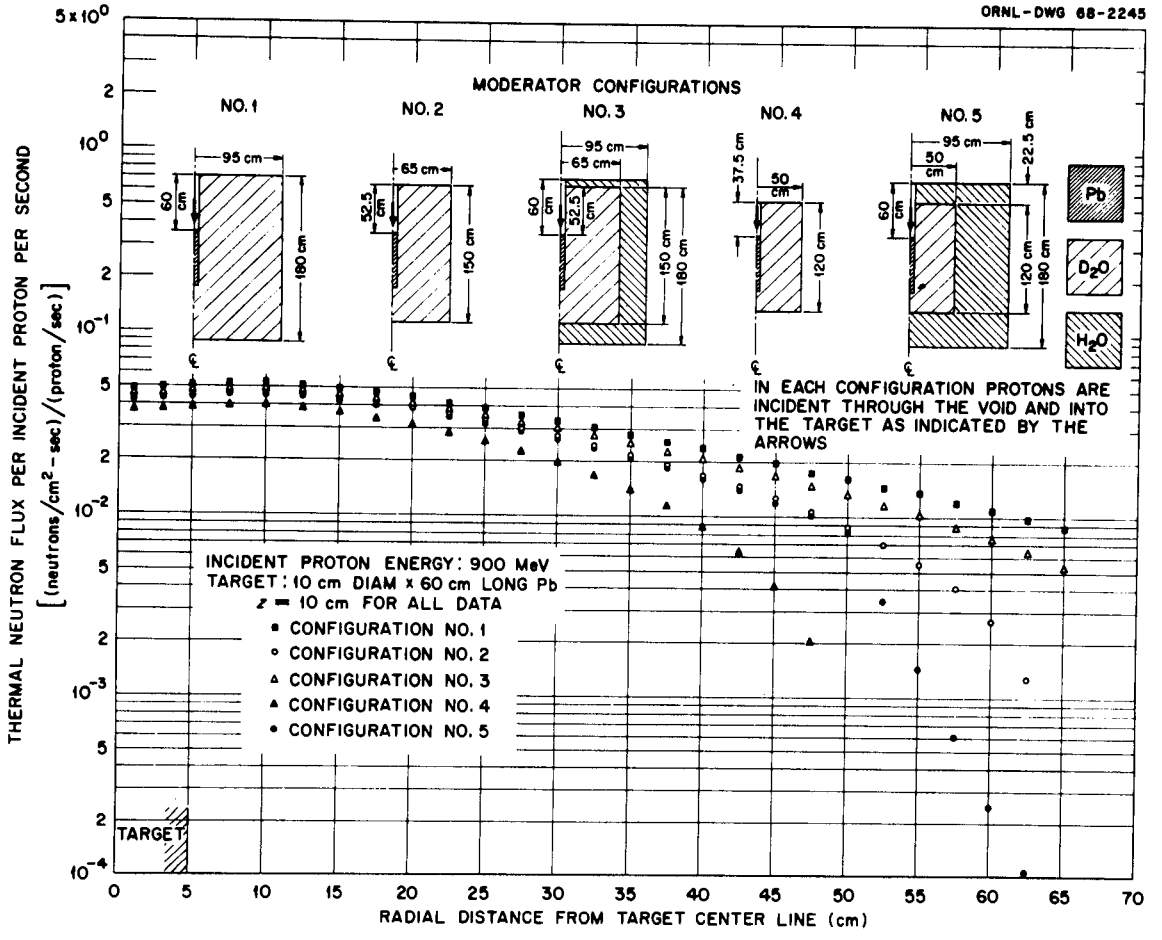

Figure 23. Comparisons of radial thermal-neutron-flux distributions at z = 10 cm using a Pb target for various moderator configurations.

source was 20.6 neutrons per incident proton. Of these neutrons 18.3 leaked from the system. In contrast, the thermal leakage in configuration No. 3 was 0.497 out of 20.3 source neutrons per incident proton. The D_2O has been reduced to 50-centimeter radius by 120 centimeters long in configuration No. 4. This is a D_2O volume reduction of 82 per cent from configuration No. 1. In configuration No. 5 an H_2O reflector has been added to the bare D_2O in configuration No. 4. The integrated thermal-neutron source in the last configuration was 20.4 neutrons per incident proton, of which only 0.052 neutrons leaked from the system. The data presented here may prove very helpful in making a cost determination of a moderator and reflector-shield design for an ING.

BIBLIOGRAPHY

BIBLIOGRAPHY

Barkas, W. H., and M. J. Berger, Tables of Energy Losses and Ranges of Heavy Charged Particles (National Aeronautics and Space Administration Report, NASA SP-3013, 1964).

Bertin, M. C., et al., Neutron Cross Sections of U^{238}, U^{235}, U^{237}, U^{239}, U^{234}, U^{236}, Pu^{239}, Pu^{240}, W, Pb, Ni, Cr, C, Li^{6}, Li^{7}, and I (United Nuclear Corporation Report, UNC-5099, 1964).

Bertini, H. W., Monte Carlo Calculations on Intranuclear Cascades (Oak Ridge National Laboratory Report, ORNL-3383, 1963).

Bertini, H. W., Preliminary Data from Intranuclear-Cascade Calculations of 0.75-, 1-, and 2-GeV Protons on Oxygen, Aluminum, and Lead, and 1-GeV Neutrons on the Same Elements (Oak Ridge National Laboratory Report, ORNL-TM-1996, 1967).

Bertini, H. W., "Intranuclear Cascade Calculations for Incident Particle Energies from 25 to 350 MeV and from 25 MeV to 2 GeV," Neutron Physics Division Annual Progress Report for Period Ending August 1, 1963 (Oak Ridge National Laboratory Report, ORNL-3499, Vol. II, 1963).

Blatt, J. M., and V. E. Weisskopf, Theoretical Nuclear Physics. New York: John Wiley and Sons, 1952.

Buckingham, B. R. S., K. Parker, and E. D. Pendlebury, Neutron Cross-Sections of Selected Elements and Isotopes for Use in Neutronics Calculations in the Energy Range 0.025 eV - 15 MeV (United Kingdom Atomic Energy Authority, Atomic Weapons Research Establishment Report No. O-28/60, 1961).

Coleman, W. A., Nucl. Sci. Eng. 32, 76-81 (1968).

Doherty, G., Neutron Cross-Sections of Be9 in the Energy Range 1 MeV to 15 MeV (United Kingdom Atomic Energy Authority Report, AEEW-M 513, 1965).

Dresner, L., EVAP - A FORTRAN Program for Calculating the Evaporation of Various Particles from Excited Compound Nuclei (Oak Ridge National Laboratory Report, ORNL-TM-196, 1961).

Fowler, T. B., M. L. Tobias, and D. R. Vondy, EXTERMINATOR-2: A FORTRAN IV Code for Solving Multigroup Neutron Diffusion Equations in Two Dimensions (Oak Ridge National Laboratory Report, ORNL-4078, 1967).

Fraser, J. S., "The Intense-Neutron-Generator Target," The AECL Symposium on The Generation of Intense Neutron Fluxes, Chalk River, Ontario, 22-23 April 1965 (Atomic Energy of Canada Limited Report, AECL-2177, 1965).

Fraser, J. S., et al., Phys. Can. 21, No. 2, 17 (1965).

Glasstone, S., and M. C. Edlund, The Elements of Nuclear Reactor Theory. New York: D. Van Nostrand Company, Inc., 1952.

Hofstadter, R., Rev. Mod. Phys. 28, 214 (1956).

Hughes, D. J., and J. A. Harvey, Neutron Cross Sections (Brookhaven National Laboratory Report, BNL-325, 1958).

Irving, D. C., R. M. Freestone, Jr., and F. B. K. Kam, 05R, A General-Purpose Monte Carlo Neutron Transport Code (Oak Ridge National Laboratory Report, ORNL-3633, 1965).

Irving, D. C., and J. Gillen, "Evaluated Cross-Section Library," Neutron Physics Division Annual Progress Report for Period Ending May 31, 1966 (Oak Ridge National Laboratory Report, ORNL-3973, Vol. I, 1966).

Joanou, G. D., and C. A. Stevens, Neutron Cross Sections for Beryllium (General Atomic Report, GA-5905 [NASA CR-54262], 1964).

Kalos, M. H., H. Goldstein, and J. Ray, Revised Cross Sections for Neutron Interactions with Oxygen and Deuterium (Nuclear Defense Laboratory Report, NDL-TR-40, 1962).

Kinney, W. E., The Nucleon Transport Code, NTC (Oak Ridge National Laboratory Report, ORNL-3610, 1964).

Lindenbaum, S. J., and R. M. Sternheimer, Phys. Rev. 105, 1874 (1957).

_____. Phys. Rev. 109, 1723 (1958).

_____. Phys. Rev. 123, 333 (1961).

Rossi, Bruno, High-Energy Particles, p. 63 ff. Englewood Cliffs: Prentice-Hall, Inc., 1952.

Webster, J. W., Point-Set Representation of ^{238}U Cross Sections; Values and a Fortran Program for Computation (Oak Ridge National Laboratory Report, ORNL-TM-1448, 1966).

Weisskopf, V., Phys. Rev. 52, 295 (1937).

Zabel, C. W., Reports to the AEC Nuclear Cross Sections Advisory Group, Idaho Falls, Idaho, July 17-18, 1957 (Nuclear Cross Sections Advisory Group, AEC, Report, WASH-194, 1958).

ACKNOWLEDGMENT

I wish to acknowledge gratefully the guidance of my advisor, Dr. R. G. Alsmiller, Jr., who was always available to assist me during the writing of this dissertation. Appreciation is extended to Dr. H. W. Bertini, Mrs. Arline Culkowski, and Mrs. Miriam Guthrie for their able and willing advice on incorporating the intranuclear-cascade program into NMTC.

I would like to thank the Oak Ridge National Laboratory, which is operated by the Union Carbide Corporation for the U. S. Atomic Energy Commission, for the use of its facilities.

I am indebted to the U. S. Atomic Energy Commission for granting the Nuclear Engineering Department a Nuclear Engineering Department-Atomic Energy Commission Traineeship, which was awarded to me. Much of the work for my dissertation was supported by this traineeship.

Finally, I wish to acknowledge my wife, Barbara, who has endured more than I during the work and writing of this dissertation.

NASA-High Energy Listing

Tino Ahrens, Advanced Research Corporation, 715 Miami Circle, N.E., Atlanta, Georgia 30324

Louis Avrami, Explosives Laboratory, Bldg. 407, Pictinny Arsenal, Dover, New Jersey 07301

M. Awschalom, Princeton Penn. Accelerator, P. O. Box 682, Princeton, New Jersey 08540

M. Barbier, CERN, Geneva Switzerland

N. Barr, Radiological Physics Branch, Division of Biology and Medicine, U. S. Atomic Energy Commission, Washington, D. C. 20545 (5 copies)

C. K. Bauer, Dept. 72-34, Z-26, Lockheed-Georgia Company, Marietta, Georgia 30060

P. R. Bell, TH, Chief of Lunar and Earth Sciences Division, Manned Spacecraft Center- NASA, Houston, Texas 77058

S. Bresticker, Grumman Aircraft Engineering Corp., Space Sciences Group, Plant 5, Bethpage, L. I., New York 11714

Karan O. Brien, Health and Safety Laboratory, Radiation Physics Division, 376 Hudson Street, New York, New York 10014

Brooks Air Force Base, Radiobiology Department, Chief, San Antonio, Texas 78235

M. O. Burrell, M-RP-NIP, National Aeronautics and Space Adm., Marshall Space Flight Center, Huntsville, Alabama 35812

B. W. Colston, U. S. Atomic Energy Commission, Sandia Area Office, P. O. Box 5400, Albuquerque, New Mexico 87115

R. G. Cochran, Department of Nuclear Engineering, A and M College of Texas, College Station, Texas

Ted Colvin, Bendix Systems Division, 3300 Plymouth Road, Ann Arbor, Michigan 48105

E. A. Cosbie, Argonne National Laboratory, Argonne, Illinois 60440

Frederick P. Cowan, Brookhaven National Laboratory, Upton, L. I., New York 11973

Director, Defense Atomic Support Agency, Pentagon, Washington, D. C. 20301

Charles A. Dempsey, 6570 AMRL (MRT), Wright-Patterson AFB, Ohio 45433

H. DeStaebler, Jr., Stanford Linear Accelerator Center, Stanford University, Stanford, California 94305

Herman J. Donnert, U. S. Army Nuclear Defense Laboratory, AMXND-C, Edgewood Arsenal, Maryland 21010

D. W. Drawbaugh, Westinghouse Electric Corp., Astronuclear Laboratory, P. O. Box 10864, Pittsburgh, Pennsylvania 15236

John E. Duberg, National Aeronautics and Space Adm., Langley Research Center, Langley Field, Virginia 23365

D. L. Dye, The Boeing Company, Mail Stop S3-72, Seattle, Washington 98124

Ronald F. Edge, Department of Physics, University of South Carolina, Columbia, South Carolina

Nat Edmunson, Code R-RP-N, National Aeronautics and Space Adm., Marshall Space Flight Center, Huntsville, Alabama 35812

Robley D. Evans, Professor of Physics, Room 6-315, Massachusetts Institute of Technology, Cambridge, Massachusetts 02139

E. M. Finkelman, Grumman Aircraft Engineering Corp., LEM Project, Plant 25, Bethpage, L.I., New York 11714

Trutz Foelsche, National Aeronautics and Space Adm., Langley Research Center, Langley Field, Virginia 23365

R. E. Fortney, Northrop Space Laboratories, 3401 West Broadway, Hawthorne, California 90250

Leo Fox, Code RBH, Biotechnology and Human Research Division, National Aeronautics and Space Adm., Washington, D. C. 20546

Stan Freden, Aerospace Corp., Box 95085, Los Angeles, California 90045

J. Y. Freeman, Division MPS, CERN, Geneva 23, Switzerland

J. Geibel, CERN, Geneva, Switzerland

R. C. Good, Jr., General Electric Company, Room M7023H - VFSTC, P. O. Box 8555, Philadelphia, Pennsylvania 19101

F. Gordon, Code 716, National Aeronautics and Space Adm., Goddard Space Flight Center, Greenbelt, Maryland 10027

Raymond M. Hansen, MS 235, National Aeronautics and Space Adm., Langley Research Center, Mail Stop 235, Langley Field, Virginia 23365

Harry Harrison, Code RRE, National Aeronautics and Space Adm., Hdqts., Washington, D. C. 20546

Russell Heath, Phillips Petroleum Company, P. O. Box 2067, Idaho Falls, Idaho 83401

Herbert D. Hendricks, National Aeronautics and Space Adm., Langley Research Center, MS499, Langley Field, Virginia 23365

W. N. Hess, National Aeronautics and Space Adm., Goddard Space Flight Center, Greenbelt, Maryland 20771

R. H. Hilberg, Bellcomm, Inc., 1100 17th Street, N.W., Washington, D. C. 20036

Charles W. Hill, Dept. 73-69, Zone 280, Lookheed-Georgia Company, Marietta, Georgia 30060

L. Hoffman, CERN, Geneva, Switzerland

J. T. Holloway, Grants and Research Contracts, Office of Space Sciences, National Aeronautics and Space Adm., Washington, D. C. 20546 (5 copies)

William C. Hulten, National Aeronautics and Space Adm., Mail Stop 235, Langley Research Center, Langley Field, Virginia 23365

T. Inada, National Institute Radiological Sciences, 250 Kurosuna-Cho, Chiba-Shi, JAPAN

Lt. Joseph F. Janni,WLRB-1, Air Force Weapons Laboratory, Kirtland Air Force Base, New Mexico 87117

Dale W. Jenkins, Chief, Environmental Biology, Office of Space Sciences, NASA, Washington, D. C. 20546

Philippe Tardy-Joubert, Serv. De Protection Contre Les Radiation, Centre D. Etudes Nucleaires De Saclay, B. P. No. 2, Gif-Sur-Yvette (Seine et Oise), FRANCE

Clyde Jupiter, General Atomic, P. O. Box 608, San Diego, California 92112

Irving Karp, NASA/ Lewis Research Center, Cleveland, Ohio 44135

Ludwig Katz, Air Force Cambridge Research Center, L. G. Hanscom Field, Massachusetts

Glenn Keister, Boeing Airplane Company, Aerospace Division, P. O. Box 3707, Seattle, Washington 98124

J. Warren Keller, Code RV-1, National Aeronautics and Space Adm., Washington, D. C. 20546 (3 copies)

James F. Kenny, Boeing Scientific Research Laboratory, P. O. Box 3981, Seattle, Washington 98124

E. C. Kidd, Zone S71, Dept. 61-2, General Dynamics/Fort Worth, P. O. Box 748, Fort Worth, Texas 76101

David King, Department of Physics, University of Tennessee, Knoxville, Tennessee 37916

Robert L. Kloster, McDonnell Aircraft Corp., P. O. Box 516, St. Louis, Missouri 63166

George A. Kolstad, Assistant Director Physics-Math Programs, Division of Research, U. S. Atomic Energy Commission, Washington, D. C. 20545

Eugene B. Konecci, Department of Management BEOB-200, University of Texas, Austin, Texas 78712

W. Kreger, Code 940, U. S. Naval Radiological Defense Laboratory, San Francisco, California 94135

Ed Kuhn, Republic Aviation Corporation, Power Conversion Systems Division, Farmingdale, L. I., New York 11735

Wright H. Langham, Los Alamos Scientific Laboratory, Los Alamos, New Mexico 87544

Borje Larsson, University of Uppsala, The Gustaf Werner Institute, Uppsala, Sweden

J. M. Lavie, Centre D. Etudes Nucleaires, De Saclay, S. E. C. R. - B. P. No. 2, 91-Gif-Sur-Yvette, FRANCE

Martin Leimdorfer, Industri-Matematik AB, De Geersgatan 8, Stockholm No. SWEDEN

S. H. Levine, Northrop Space Laboratories, 3401 W. Broadway, 2452/61, Hawthorne, California 90250

Lynn R. Lewis, Dept. 250, Bendix Systems Division, 3300 Plymouth Road, Ann Arbor, Michigan 48105

John R. Lilley, A-830-BBFO-78, Missile Space Systems Division, Douglas Aircraft Co., Inc., Santa Monica, California

S. J. Lindenbaum, Brookhaven National Laboratory, Upton, L. I., New York 11973

Major Russell E. Linkous, Air Force Systems Command (SCTR), Andrews AFB, Maryland 20331

M. Stanley Livingston, Cambridge Electron Accelerator, 42 Oxford Street Cambridge, Massachusetts 02139

Robert Macklin, Jet Propulsion Laboratory, Pasadena, California 91103

Brian Mar, Boeing Airplane Co., MS 23-82, Aerospace Division, P. O. Box 3707, Seattle, Washington 98124

Thomas J. McGuire, Systems Engineering Group (SESSV), Wright-Patterson AFB, Ohio 45433

E. J. McLaughlin, Space Medicine, NASA - Code MM, Washington, D. C. 20546

R. V. Meghreblian, Jet Propulsion Laboratory, 4800 Oak Grove Drive, Pasadena, California 91103

Albert E. Metzger, Jet Propulsion Laboratory, 354-401F, 4800 Oak Grove, Pasadena, California

J. M. Miller, Chemistry Department, Columbia University, New York, New York 10027

R. A. Miller, Zone S71, Dept. 61-2, General Dynamics/Fort Worth, P. O. Box 748, Fort Worth, Texas 76101

Jerry L. Modisette, National Aeronautics and Space Adm., Manned Spacecraft Center, Houston, Texas 77001 (5 copies)

Winnie M. Morgan, Technical Reports, Grants and Research Contracts, Office of Space Sciences, NASA, Washington, D. C. 20546 (25 copies)

B. J. Moyer, University of California, Lawrence Radiation Laboratory, 6141 Building 50A, Berkeley, California 94720

R. F. Mozley, SLAC, Stanford University, Stanford, California 94305

Capt. J. D. Munson, Space Systems Division (SSTDS), Los Angeles Air Force Station, Los Angeles, California 90045

Sam V. Nablo, ION Physics Corporation, Burlington, Massachusetts 01803

R. R. Nash, Code RRM, National Aeronautics and Space Adm., Washington, D. C. 20546

John P. Neissel, MC-506, 175 Courtner Avenue, General Electric Company, San Jose, California 95125

W. R. Nelson, Stanford Linear Accelerator Center, Stanford, California 94305

W. K. H. Panofsky, Stanford Linear Accelerator Center, Stanford University, Stanford, California 94305

Wade Patterson, University of California, Lawrence Radiation Laboratory, Berkeley, California 94720

Maynard Pearson, Boeing Airplane Company, Aerospace Division, P. O. Box 3707, Seattle, Washington 98124

Col. John E. Pickering, USAF, National Aeronautics and Space Adm., (Code MM), Washington, D. C. 20546

G. F. Pieper, Code 600, National Aeronautics and Space Adm., Goddard Space Flight Center, Greenbelt, Maryland 10027

Robert Pruett, P. O. Box 95085, Los Angeles, California 90045

Arthur Reetz, Code RV-1, National Aeronautics and Space Adm., Washington, D. C. 20546 (3 copies)

O. Reynolds, Director, Bio-Science Programs, Office of Space Sciences, National Aeronautics and Space Adm., Washington, D. C. 20546 (5 copies)

Robert G. Riedesel, Douglas Aircraft Company, Missile and Space Division, 3000 Ocean Park Blvd., Santa Monica, California 90405

Don Robbins, ET32, National Aeronautics and Space Adm., Manned Spacecraft Center, Houston, Texas 77058

H. J. Schaefer, U. S. Naval School of Aviation Medicine, U. S. Naval Aviation Medical Center-54, Pensacola, Florida 32512

W. Wayne Scott, Chattanooga State Technical Institute, 4501 Amnico Highway, Chattanooga, Tennessee 37401

Robert L. Seale, University of Arizona, Tuscon, Arizona 85721

Pierre Lafore Sepp, Commissariat A L. Energie Atomique, Centre D. Etudes Nucleaires, De Fontenay-Aux-Roses (Seine), Boite Postale No. 6, 92 Fontenay Aux Roses, FRANCE

Jerome L. Shapiro, Division Engineering and Applied Science, Pasadena, California 91109

R. D. Shelton, Code R-RP-N, National Aeronautics and Space Adm., Marshall Space Flight Center, Huntsville, Alabama

Robert T. Siegel, Department of Physics, College of William and Mary, Williamsburg, Virginia 23185

J. J. Singh, M.S. 234, NASA. Langley Research Center, Langley Station, Hampton, Virginia 23365

G. D. Smith, Ames Research Center, Moffett Field, California 94035

Jerry Speakman, 6570 AMRL (MRBBR), Wright-Patterson AFB, Ohio

Dwain F. Spencer, Jet Propulsion Laboratory, Pasadena, California 31103

Stanford Linear Accelerator Center, ATTN: Library, P. O. Box 4349, Stanford, California 94305

William Steigelmann, Kuljian Corp., 1200 North Broad Street, Philadelphia, Pennsylvania 19121

Henry Stern, R-RP-N, NASA, Marshall Space Flight Center, Huntsville, Alabama 35812

T. R. Strayhorn, S-71, General Dynamics, Fort Worth, Texas 76101

S. Tom Taketa, Mail Stop N 236-5, NASA, Ames Research Center, Moffett Field, California 94035

Eizo Tajima, Rikkyo University, Ikebukuro, Toshimaku, Tokyo, JAPAN

Ralph H. Thomas, Rutherford High Energy Laboratory, Chilton, Didcot, Berks, ENGLAND

O. Lyle Tiffany, Chief Scientist, Bendix Systems Division, 3300 Plymouth Road, Ann Arbor, Michigan 48103

Cornelius Tobias, University of California, Lawrence Radiation Laboratory, Berkeley, California 94720

Jacob I. Trombka, Code SM, National Aeronautics and Space Adm., Washington, D. C. 20546

W. Turchinetz, Massachusetts Institute of Technology, 155 Massachusetts Avenue, Cambridge, Massachusetts

Werner Von Braun, Director, George C. Marshall Space Flight Center, NASA, Huntsville, Alabama 35812

G. P. Wachtell, Franklin Institute, 20th and Parkway, Philadelphia, Pennsylvania 19103

Roger Wallace, University of California, Bldg. 72, Lawrence Radiation Laboratory, Berkeley, California 94720

G. T. Western, Y-71, General Dynamics, Fort Worth, Texas 76101

Glenn A. Whan, Associate Professor, Nuclear Engineering Laboratory, The University of New Mexico, Albuquerque, New Mexico 87106

Robert V. Wheeler, R. S. Landauer, Jr. and Co., 3920 216th Street, Matteson, Illinois 60443

Ralph Wiley, Mail Zone Y-42, P. O. Box 748, Fort Worth, Texas 76101

Maurice Wilkinson, The Boeing Company, M. S. 23-82, Seattle, Washington 98124

W. R. Yucker, A-2-833, Douglas Aircraft Co., Nuclear Department, 3000 Ocean Park Boulevard, Santa Monica, California 90405

Marcello Zocchi, Reactor and Radiation, National Bureau of Standards, Washington, D. C. 20234

K. Ziock, Department of Physics, University of Virginia, Charlottesville, Virginia 32901

J. Scanlon, Research Department, Grumman Aircraft Engineering Corp., Bethpage, New York 11714

Donald W. Aitken, Research Physicist, Stanford University, Department of Physics, Stanford, California

Wayne A. Coleman, Box 856, Edgewood, Maryland 21040 (10 copies)

TM-2206

INTERNAL DISTRIBUTION

1-2. L. S. Abbott
3. A. Zucker
4. F. Alsmiller
5. R. G. Alsmiller, Jr.
6. T. Armstrong
7. H. Bertini
8. C. E. Clifford
9. T. A. Gabriel
10. E. E. Gross
11. M. Guthrie
12. D. C. Irving
13. D. F. King
14. W. E. Kinney
15. R. S. Livingston
16. T. A. Love
17-18. F. C. Maienschein
19. R. W. Peelle
20. F. G. Perey
21. A. M. Perry
22. R. T. Santoro
23. G. de Saussure
24. D. Sundberg
25. D. K. Trubey
26. J. W. Wachter
27. W. Zobel
28. M. H. Kalos (consultant)
29. E. R. Cohen (consultant)
30. B. C. Diven (consultant)
31. W. N. Hess (consultant)
32. L. V. Spencer (consultant)
33-34. Central Research Library
35. Document Reference Section
36-50. Laboratory Records Department
51. Laboratory Records ORNL RC
52. ORNL Patent Office

EXTERNAL DISTRIBUTION

53. P. B. Hemmig, Division of Reactor Development and Technology, U. S. Atomic Energy Commission, Washington, D. C.
54. Graham P. Stevenson, Rutherford High Energy Laboratory, Chilton, Didcot, Berkshire, England.
55. I. F. Zartman, Division of Reactor Development and Technology, U. S. Atomic Energy Commission, Washington, D. C.
56. High Energy Preprint Library, Department of Physics, University of Toronto, Toronto 5, Ontario, Canada.
57-200. Given NASA-High Energy Distribution listed on preceding pages.
201-215. Division of Technical Information Extension (DTIE)
216. Laboratory and University Division, ORO